Biogeochemical Impact of Cable Bacteria on Coastal Black Sea Sediment

Martijn Hermans[1], Nils Risgaard-Petersen[2,3], Filip J.R. Meysman[4,5] and Caroline P. Slomp[1]

[1]Department of Earth Sciences, Faculty of Geosciences, Utrecht University, P.O Box 80021, 3508 TA Utrecht, the Netherlands

[2]Center for Geomicrobiology, Section for Microbiology, Department of Bioscience, Aarhus University, Aarhus, Denmark

[3]Center for Electromicrobiology, Section for Microbiology, Department of Bioscience, Aarhus University, Aarhus, Denmark

[4]Center of Excellence for Microbial Systems Technology, Department of Biology, University of Antwerp, Wilrijk, Belgium

[5]Department of Biotechnology, Delft University of Technology, Delft, the Netherlands

ABSTRACT

Cable bacteria can strongly alter sediment biogeochemistry. Here, we used laboratory incubations to determine the potential impact of their activity on the cycling of Fe, phosphorus (P) and sulphur (S). Microsensor depth profiles of oxygen, sulphide and pH in combination with electric potential profiling and FISH analyses showed a rapid development (<5 days) of cable bacteria, followed by a long period of activity (>200 days). During most of the experiment, the current density correlated linearly with the oxygen demand. Sediment oxygen uptake was attributed to activity of cable bacteria and the oxidation of reduced products from anaerobic degradation of organic matter, such as ammonium. Pore water sulphide was low (<5 μM) throughout the experiment. Sulphate reduction acted as the main source of sulphide for cable bacteria. Pore water Fe^{2+} reached levels of up to 1.7 mM during the incubations, due to the dissolution of FeS (30%) and siderite, an Fe carbonate mineral (70%). Following upward diffusion of Fe^{2+}, a surface enrichment of Fe oxides formed. Hence, besides FeS, siderite may act as a major source of Fe for Fe oxides in coastal surface sediments where cable bacteria are active. Using μXRF, we show that the enrichments in Fe oxides induced by cable bacteria are located in a thin subsurface layer of 0.3 mm. We show that similar subsurface layers

enriched in Fe and P are also observed at field sites where cable bacteria were recently active and little bioturbation occurs. This suggests that such subsurface Fe oxide layers, which are not always visible to the eye, could potentially be a marker for recent activity of cable bacteria.

Key words: cable bacteria, elemental cycling, solute fluxes, iron

1. INTRODUCTION

Depletion of oxygen (O_2) in bottom waters (i.e. water directly above the seafloor) of coastal areas is increasing worldwide, as a consequence of eutrophication and climate change (Diaz and Rosenberg 2008; Schmidtko et al. 2017; Breitburg et al. 2018). Low O_2 can lead to the development of coastal 'dead zones' characterised by recurrent mortality of marine life (Rabalais et al. 2002; Diaz and Rosenberg 2008). Progressive eutrophication induces a characteristic response of coastal systems with transient and seasonal hypoxia (O_2 < 63 µM) transitioning into permanent anoxia (O_2 = 0 µM). In this later stage, free sulphide (H_2S) may escape from the sediment and accumulate in the bottom water, a condition referred to as euxinia (Diaz and Rosenberg 2008; Kemp et al. 2009; Rabalais et al. 2014). As H_2S is highly toxic to higher fauna, the development of euxinia may aggravate the ecological consequences. However, the presence of iron (Fe) and manganese (Mn) oxides in surface sediments may delay this transition towards euxinia by removing H_2S and thus preventing an efflux of H_2S to the overlying water (Kristiansen et al. 2002; Kristensen et al. 2003; Diaz and Rosenberg 2008).

Cable bacteria are multicellular filamentous sulphur(S)-oxidising bacteria (Pfeffer et al. 2012) that strongly enhance the formation of Fe and Mn oxides and efficiently remove H_2S from surface sediments (Risgaard-Petersen et al. 2012; Seitaj et al. 2015; Sulu-Gambari et al. 2016a). Cable bacteria belong to the *Desulfobulbaceae* family of the Deltaproteobacteria (Trojan et al. 2016; Kjeldsen et al. 2019). Cable bacteria can spatially link the oxidation of H_2S in deeper sediments to the reduction of O_2 near the sediment-water interface by transporting electrons over centimetre scale distances (Pfeffer et al. 2012) through a conductive fibre network that is embedded in the cell envelope (Meysman et al. 2019). This spatial coupling of surficial O_2 reduction with H_2S oxidation at several centimetres depth creates a suboxic zone that is devoid of any O_2 and H_2S, and provides cable

bacteria a competitive advantage over other S-oxidising bacteria in aquatic environments (Meysman 2018). Cable bacteria have been documented in a range of fresh water (Risgaard-Petersen et al. 2015; Müller et al. 2016) and marine environments (Malkin et al. 2014; Burdorf et al. 2017), however, they appear to be particularly active in sediments overlain by seasonally hypoxic bottom waters (Seitaj et al. 2015; Burdorf et al. 2018).

The metabolic activity of cable bacteria establishes an electrical circuit in the sediment, which involves an electron current through the cable bacteria filaments (Bjerg et al. 2018), and an ionic current through the pore water in the opposite direction (Naudet and Revil 2005; Revil et al. 2010; Risgaard-Petersen et al. 2012). As a consequence, an electric potential (EP) is generated in the sediment, which can be used as a reliable indicator for activity of cable bacteria (Risgaard-Petersen et al. 2014).

Cable bacteria activity additionally generates a distinct biogeochemical signature, that can be assessed by pH, O_2 and H_2S depth profiling (Nielsen et al. 2010). Their activity leads to the development of a suboxic zone (i.e. a zone where O_2 and H_2S are both absent), and also induces a pH profile that strongly changes with depth. Cathodic O_2 reduction ($O_2 + 4H^+ + 4e^- \rightarrow 2H_2O$) in the oxic zone of the sediment results in a pH maximum (~9) due to proton consumption, whereas anodic sulphide oxidation ($H_2S + 4\ H_2O \rightarrow SO_4^{2-} + 10H^+ + 8e^-$) causes a pH minimum (<6.5) in the anoxic zone (Fig. 1A; Nielsen et al. 2010; Meysman et al. 2015).

The presence of cable bacteria in sediments can strongly impact the elemental cycling of Fe, Mn, Ca and S (Risgaard-Petersen et al. 2012; Seitaj et al. 2015; Rao et al. 2016; Sulu-Gambari et al. 2016a; van de Velde et al. 2016). Pore water acidification induced by cable bacteria activity can lead to dissolution of calcium (Ca) carbonates, Fe carbonates (siderite), Mn carbonates and FeS in the zone where the pH is low, thus generating high concentrations of Fe^{2+} and Mn^{2+} in the pore water (Risgaard-Petersen et al. 2012; Rao et al. 2016). When these dissolved species diffuse upward this can lead to strong enrichments of Fe and Mn oxides upon contact with O_2, or for dissolved Fe^{2+}, also upon contact with Mn oxides (Wang and Van Cappellen 1996; Seitaj et al. 2015; Sulu-Gambari et al.

2016a). These metal oxides are capable of efficiently buffering the benthic release of H_2S and phosphate (HPO_4^{2-}) during periods with low bottom water O_2. This so-called 'firewall' for H_2S and alteration of the timing of HPO_4^{2-} release linked to this buffering can play a key role in regulating water quality in seasonally hypoxic coastal systems (Seitaj et al. 2015; Sulu-Gambari et al. 2016b; Hermans et al. 2019a).

In coastal sediments, O_2 typically penetrates to a depth of only several mm's below the sediment-water interface (Rasmussen and Jørgensen 1992; Rabouille et al. 2003; Glud 2008). This also holds true for sediments inhabited by active cable bacteria (Nielsen et al. 2010; Pfeffer et al. 2012; Larsen et al. 2015). Hence, the oxidation of upward diffusing Fe^{2+} and Mn^{2+} is expected to take place below and not at the sediment-water interface. We hypothesise that, as a consequence, in the initial stages of cable bacteria activity and in the absence of bioturbation, most Fe and Mn oxide enrichments will be restricted to a thin subsurface layer of the sediment. However, the sample resolution and timing of the collection of solid phase data in field and laboratory studies published so far do not allow an assessment of this hypothesis.

Cable bacteria are suggested to thrive in coastal sediments characterised by high rates of H_2S production due to high rates of organic matter mineralisation (Malkin et al. 2014; Burdorf et al. 2017; Hermans et al. 2019a). Laboratory and model studies have shown that the dissolution of FeS accounts for 12 to 94% of the H_2S consumed by cable bacteria, while the other source is H_2S production from the reduction of SO_4^{2-} (Risgaard-Petersen et al. 2012; Meysman et al. 2015; Burdorf et al. 2018). At present, it is not known if cable bacteria activity can establish in sediments that are relatively low in FeS and dissolved H_2S.

In this study, we assess whether cable bacteria activity can establish and thrive in sediments that are relatively poor in FeS. Although, this will be done in a controlled incubation experiment with siderite-bearing sediments from a coastal site in the Black Sea, our findings are relevant for natural environments populated by cable bacteria. The metabolic activity of cable bacteria is monitored using microsensor profiles of pH, O_2, H_2S and EP. We also use sediment Fe and P speciation and µXRF of

resin-embedded sediments to test whether we find evidence for subsurface enrichments in Fe oxides and associated P. We find a rapid establishment of cable bacteria (<5 days) and the development of an Fe oxide-rich subsurface layer, with the majority of the Fe ~70% supplied through dissolution of siderite induced by cable bacteria activity. The depth of the Fe oxide layer was directly related to the O_2 penetration depth and we propose that such subsurface enrichments in Fe, which also can contain P and Mn, can be used as a marker for recent cable bacteria activity.

2. METHODS AND MATERIALS

2.1. Study Area and Experimental Set-up

In September 2015, 16 sediment cores (⌀10 cm) were retrieved at a coastal site on the north-western shelf of the Black Sea (27 m water depth; Fig. 1B; Table 1) using a multicorer (Oktopus GmbH, Germany) as described in Lenstra et al. (2019). The overlying water was discarded, and the upper 10 cm of the sediment was transferred into nitrogen purged aluminium bags that were sealed and stored at 4 °C for several months. The anoxic storage is expected to have led to the death of all macrofauna and most meiofauna (Coull and Chandler 2001; Riedel et al. 2012). Prior to incubation, the sediment was passed through a 4 mm sieve to remove large debris and homogenised. Subsequently, the sediment was transferred to 18 transparent polycarbonate cores (⌀6 cm; 20 cm length).

The bottom 15 cm of these cores was filled with sediment and the upper 5 cm with overlying water. The cores were placed in two aquaria filled with artificial seawater (Instant Ocean Sea Salt + Ultra High Quality (UHQ) water) with a salinity of 17.9, identical to the bottom water salinity at the study site. The artificial sea water contained negligible concentrations of NH_4^+, NO_3^-, Fe, Mn and P as described in Atkinson (1997) and Hovanec and Coshland (2004). The aquaria were kept in the dark at a constant temperature (~20 °C), and the water was continuously aerated by two aquarium pumps. Sixteen out of eighteen cores were exposed to oxygenated overlying water in the aquaria, whereas the two remaining cores served as an anoxic control treatment. The control cores were tightly sealed with rubber stoppers, to prevent the growth of cable bacteria by excluding O_2 (Nielsen et al. 2010).

Sampling for pore water and solid-phase analyses was performed at eight time points over a total incubation period of 621 days. Each time point involved a three day procedure. On the first day, microsensor depth profiles of EP, O_2, pH and H_2S were obtained in two randomly selected oxic cores and the two anoxic control cores (O_2 profiling was not performed in the anoxic cores). On the second day, solute fluxes were measured in the same oxic cores that were used for microsensor depth profiling on the previous day. On the third day, the two cores were sectioned, of which only one core was processed further for pore water and solid-phase analyses. Photographs were taken at four time points (day 12; 33; 170 and 621) from one oxic core to follow the visual development of the surface sediment during the experiment.

2.2. High-resolution Microsensor Depth Profiling

High-resolution depth profiles of pH, O_2 and H_2S were obtained (50-µm depth resolution; 3 replicate profiles per oxic core; 2 replicate profiles per anoxic core) using commercial micro electrodes (Unisense A.S., Denmark). The O_2 sensor was re-calibrated prior to each measurement, using saturated bottom water (100% [O_2]) and the deeper sediment horizons (0% [O_2]) as calibration points. Calibrations of the pH and H_2S electrodes were performed as described in Hermans et al. (2019b). pH values are reported on the total scale. For depth profiling of EP (500-µm resolution; 3 replicates per core), micro electrodes were used that were custom built at Aarhus University, as described in Damgaard et al. (2014). A robust reference electrode (Ref-RM, Unisense, A.S., Denmark) was used during EP and pH measurements. To exclude turbulence-induced variations in the potential of the reference electrode during EP profiling, a silicon tube filled with foam was mounted on the tip of the reference electrode.

2.3. Solute Flux Measurements

Solute flux incubations were performed for NH_4^+, Fe^{2+}, Mn^{2+}, Ca^{2+}, HPO_4^{2-} and H_4SiO_4. At each time point, one core was placed outside the aquarium at 20 °C, and the isolated volume of overlying water in the core was continuously aerated. Potential stratification of the overlying water was prevented by actively bubbling it. Parafilm was wrapped on top of the cores to prevent evaporation. Water samples of 3 mL were retrieved at 7 time points over 24 hours. The same volume

of fresh artificial seawater was added to the cores directly after taking each sample. The samples were filtered (0.45 μm), and subsamples were taken for ammonium (1 mL) and for metals (1 mL; acidified with 10 μL Suprapur® HCl (35%) per mL sample), which were stored at -20°C and 4°C respectively until further analysis.

2.4. Pore Water and Sediment Collection

At each time point, two cores were sectioned at 0.5-1 cm resolution with an UWITEC push-up pole in a nitrogen-purged glovebag, but only samples for one core were used for sediment and pore water collection and analyses. Bottom water samples were retrieved from the overlying water in the cores. Slices for each depth interval were centrifuged at 3500 rpm for 20 minutes for pore water retrieval. Samples (1 mL) for NH_4^+ were taken and stored at -20°C until analysis. Samples (1 mL) for pore water S, Fe, Mn, Ca, P and Si were also collected and acidified with 10 μL Suprapur® HCl (35%) per mL sample, which were stored at 4°C until analysis. Centrifuged sediment samples were freeze-dried and ground to a fine powder in a nitrogen-purged glovebox under a strictly anoxic environment to prevent oxidation (Kraal et al. 2009; Kraal and Slomp 2014). Only the top 5 cm of the solid-phase samples were analysed in further detail. The porosity (Supporting Information 1.1; Table S1) was calculated from the weight loss upon freeze-drying, using a sediment density of 2.65 g cm^{-3} (Burdige 2006). Salt corrections were performed on the solid-phase data using the gravimetric water content and salinity to determine the amount of salt after freeze-drying. After freeze-drying, the salt from seawater stays behind in the solid-phase fraction. To determine the actual weight of the dry sediment, it is necessary to subtract the weight of the salt from the total weight of freeze-dried sediment.

2.5. Chemical Analysis of the Water and Sediment

Concentrations of NH_4^+ in the pore water and solute flux samples were determined using the phenol hypochlorite method (Koroleff 1969). The total Fe, Mn, Ca, P and Si concentrations (which are assumed to represent Fe^{2+}, Mn^{2+}, Ca^{2+}, HPO_4^{2-} and H_4SiO_4) in the pore water and solute flux samples were determined using Inductively Coupled Plasma-Optical Emission Spectroscopy (ICP-OES, Spectro Arcos). Dissolved Fe and Mn are assumed to be present in the form of Fe^{2+} and Mn^{2+},

however some Mn^{3+} (Madison et al. 2013) or colloidal and nanoparticulate Fe and Mn might also be available (Boyd and Ellwood 2010; Raiswell and Canfield 2012). Concentrations of P and S are assumed to represent HPO_4^{2-} and SO_4^{2-} respectively. The colourimetric detection limit for NH_4^+ was 0.5 μM. The practical detection limit on the ICP-OES for Fe, Mn and P was 0.73, 0.11 and 7.30 μM, respectively.

Solid-phase Fe was fractionated into [1] labile ferric Fe (hydr)oxides and ferrous Fe (FeS + $FeCO_3$), [2] crystalline Fe minerals, [3] magnetite and [4] pyrite (Supporting Information 1.2; Table S2), using a combination of two operational extraction methods (Poulton and Canfield 2005; Claff et al. 2010) as described by Kraal et al. (2017). Concentrations of Fe in all extracts were determined using the colourimetric phenanthroline method (APHA 2005). Solid-phase S was separated into [1] acid volatile sulphur (AVS; representing FeS) and [2] chromium reducible sulphur (CRS; representing FeS_2; Table S1) using the method after Burton et al. (2006; 2008) as modified by Kraal et al. (2013). Sulphide released during the S extraction was trapped as ZnS in alkaline Zn acetate traps. Concentrations of S were determined by iodometric titration (APHA 2005). Solid-phase siderite ($FeCO_3$) was determined by subtracting AVS from the labile ferrous concentrations retrieved from the first step of the Fe extraction. Solid-phase P was fractionated into [1] exchangeable P, [2] citrate-dithionite-bicarbonate (CDB)-P, [3] authigenic P, [4] detrital P and [5] organic P (Table S2) after Ruttenberg (1992) as modified by Slomp et al. (1996). The sum of exchangeable P and CDB-P represents metal bound P, as described in Hermans et al. (2019b). Concentrations of P in all extracts, except CDB, were measured with the molybdenum blue colourimetric method (Murphy and Riley 1958). The P, Mn (assuming to represent Mn oxides; Hermans et al. 2019b) and Si (assuming to represent metal oxide bound Si; Kostka and Luther III 1994; Rao et al. 2016) in CDB extracts was determined using ICP-OES.

2.6. Elemental Mapping of Fe, Mn, P and Ca

On day 47, an undisturbed core (first 5 cm of surface sediment) was sampled for epoxy resin embedding for high-resolution elemental mapping (Jilbert et al. 2008; Jilbert and Slomp 2013). Sediment was carefully pushed upwards from the experimental core into a shorter (7 cm length; 1 cm

diameter) mini core. This mini sub-core was then transferred to an acetone bath in a argon-filled glovebox and subsequently embedded with Spurr's epoxy resin as described in Jilbert et al. (2008). After curing, the epoxy-embedded core was split vertically using a rock saw. The surface was smoothed by applying a 0.3 µm alumina powder layer. Elemental maps of Fe, Mn, P and Ca (30 µm resolution) were retrieved using a Desktop EDAX Orbis µXRF analyser (Rh tube set at 30 kV, 500 µA, 300 ms dwell-time, equipped with a poly-capillary lens). Similar µXRF maps for Fe, Mn and P in epoxy embedded surface sediment were obtained for two field sites: (1) the Gulf of Finland, for sediments collected in June 2016 as described by Hermans et al. (Submitted), and Lake Grevelingen, for sediments collected in January and May 2012 as described in Sulu-Gambari et al. (2016a; 2018).

2.7. Fluorescence *In-situ* Hybridisation

Fluorescence *in-situ* hybridisation (FISH; Pernthaler et al. 2001) was used to microscopically quantify the abundance of cable bacteria filaments, as described in Seitaj et al. (2015). FISH analysis was performed on one intact sediment core retrieved at our sampling site, and the sediment cores from our incubation experiment used for pore water collection at three time points (days 5, 26 and 207). These cores were sectioned at 0.5 cm depth resolution for the first 2.5 cm. Each sediment slice was homogenised and fixed with 0.5 mL ethanol (≥99.8% purity), and stored in a 2 mL Eppendorf tube at -20 °C. For FISH analysis, a volume of 100 µL was retrieved from the Eppendorf tubes and mixed with a 1:1 solution of PBS/ethanol (500 µL). Then 10 µL of this mixture was filtered through a polycarbonate membrane (type GTTP; pore size 0.2 µm, Millipore, USA). Cable bacteria were classified with a *Desulfobulbaceae*-specific oligonucleotide probe (DSB706; 5-ACC CGT ATT CCT CCC GAT-3') after counter staining with DAPI (1 µg/mL) under an epifluorescence microscope (Zeiss Axioplan, Germany) at 100x magnification. The abundance of cable bacteria was quantified by determining the length and diameter of all observed filaments in a field (105 × 141 µm) on the filter at 100x magnification (200 fields per sample). Cable bacterial abundances are expressed as filament length per volumetric unit (m cm^{-3}) or depth integrated per unit area of sediment surface (m cm^{-2}), consistent with previous studies (Schauer et al. 2014; Malkin et al. 2017).

2.8. Scanning Electron Microscopy

Cable bacteria filaments were taken from surface sediments from the oxic zone (upper 2 mm) after 40 days using a microscope and were transferred to a 15 mL centrifuge tube. The tube was filled to a volume of ~10 mL using ultra clean water, and was subsequently centrifuged at 2100 rpm for 2 min, after which the water was discarded. This washing step was repeated three times. The washed samples were then transferred to a sample stub, where the sediment was air-dried over-night prior to gold coating. The filaments were subsequently subjected to scanning electron microscopy (SEM) imaging on a Phenom ProX Desktop SEM (Phenom-World B.V., the Netherlands) to obtain high-resolution images, as described in Geerlings et al. (2019). SEM images were generated under 0.1-0.3 mbar vacuum, and a high accelerating voltage (10 or 15 kV).

2.9. Data Analysis and Calculations

The diffusive uptake of O_2 was calculated from the high-resolution O_2 depth profiles using the PROFILE software package (Berg et al. 1998). Total H_2S ($\Sigma H_2S = H_2S + HS^- + S^{2-}$) was calculated as a function of the recorded H_2S and pH values, accounting for temperature and salinity (Millero et al. 1988; Jeroschewski et al. 1996).

The EP depth profiles were normalised by subtracting the background EP signal in the overlying water from the EP depth profiles, to calculate the EP value relative to that in the overlying water (Damgaard et al. 2014). The electric field in the sediment was calculated from the linear slope of the EP depth profiles (average of triplicates) in the surface sediments (Risgaard-Petersen et al. 2014). The magnitude of the current density was subsequently calculated from the gradient in the EP, the so-called electric field, using Ohm's law:

$$J = \sigma_{sed} \cdot E \quad (1)$$

where J represents the magnitude of the current density (mA m^{-2}), σ_{pw} is the conductivity of the sediment matrix (S m^{-1}) and E (mV m^{-1}) represents the electric field. The conductivity of the pore water was corrected for tortuosity and calculated as a function of the temperature and salinity using the equations provided by Fofonoff and Millard Jr (1983).

The solute fluxes were calculated as described in Glud (2008)and Rao et al. (2016):

$$J = \frac{\Delta C_{ow}}{\Delta t} \cdot \frac{V_{ow}}{A} \quad (2)$$

where J represents the diffusive flux (mmol m^{-2} d^{-1}), ΔC_{ow} represents the concentration change in the overlying water (mmol m^{-3}), Δt is the incubation time (d), V_{ow} is the volume in the overlying water (m^3) and A the surface area of sediment in the core (m^2). In our experimental setup, only those fluxes were measurable for NH_4^+, Fe^{2+}, Mn^{2+} and HPO_4^{2-}, that were >0.08, >0.06, >0.01 and >0.55 mmol m^{-2} d^{-1}, respectively. However, for these four solutes, fluxes were always too low to be detected. Hence, only Ca^{2+} and H_4SiO_4 fluxes are presented.

Diffusive downward fluxes of SO_4^{2-} and diffusive upward fluxes of NH_4^+, Fe^{2+}, Mn^{2+} and Ca^{2+} were calculated from linearized pore water gradients using Fick's first law (Berner 1980):

$$J = -\phi D_s \cdot \frac{dC}{dz} \quad (3)$$

The molecular diffusion coefficient was calculated as a function of pressure, salinity and temperature using the R package *marelac* (Soetaert et al. 2010) and corrected for the ambient tortuosity using the relations listed in Boudreau (1997).

3. RESULTS

3.1. Abundance of Cable Bacteria

Examination of the top 2.5 cm of the surface sediments using FISH showed the presence of filamentous cable bacteria (Fig. 1C; Fig. S1). The *in-situ* cable bacterial abundance in the sediment at our field site was low (14 m cm^{-2}). However, after 5 days of incubation in the laboratory, the abundance increased strongly (724 m cm^{-2}). At day 26 the abundance of cable bacteria was even higher (1035 m cm^{-2}). After 207 days, the cable bacterial abundance in the surface sediment was low again (131 m cm^{-2}). SEM imaging confirmed that filaments were indeed cable bacteria (Fig. 1D), as the external surface of the filament was characterised by a parallel pattern of ridges and grooves along

its latitudinal axis, which is a typical feature of cable bacteria (Cornelissen et al. 2018; Geerlings et al. 2019).

3.2. High-resolution Depth Profiles of pH, O_2 $\sum H_2S$ and EP

High-resolution depth profiles of pH showed the development of a distinct peak near the sediment-water interface at day 5, and acidification of the pore water in the deeper sediment (Fig. 2A). The width of this pore water acidification zone increased with time and reached its maximum at day 26, followed by a decrease in the acidification. The distinct pH peak near the sediment-water interface gradually disappeared after 33 days. The depth of O_2 penetration in the sediment remained constant within the first 40 days of incubation (~1.1 mm) and subsequently moved downwards with time to 9.6 mm (Fig. 2A; Fig. 3; Fig. S2). The dissolved $\sum H_2S$ concentrations remained low (<5 μM) throughout the experiment (Fig. 2A). The ΣH_2S appearance depth was initially equivalent to the O_2 penetration depth, and shifted downwards within 5 days, creating a suboxic zone where O_2 and ΣH_2S remained below detection (Fig. 2A; Fig. 3). The width of the suboxic zone remained relatively constant with time (~25 mm; Fig. 3), and only slight decreased after 207 days.

The EP depth profiles indicate a rapid establishment of an electric current after 5 days (0.4 mV; Fig. 2B). The time-series of depth profiles show that the EP increased and also accumulated over a thicker depth horizon. At day 26 the EP reached its maximum value (1.2 mV), followed by a decrease with time. Long-distance electron transport was not active in the anoxic control core (Fig. S3).

3.3. Diffusive Uptake of O_2 and Current Density

The diffusive O_2 uptake of the sediment was highest after 5 days and gradually decreased with time from ~30 to ~3.6 mmol m^{-2} d^{-1} (Fig. 4A). The current density rapidly increased from day 0 to day 18, from 6 to 128 e^- mmol m^{-2} d^{-1}, and then gradually decreased with time (Fig. 4B). The duplicate measurements show the same trend for the diffusive O_2 uptake and the current density, which indicates that the results are reproducible.

3.4. Pore Water Profiles

Concentrations of NH_4^+ were low near the sediment-water interface and increased with sediment depth reaching maximum levels of up to 1.7 mM at depth in the sediment (Fig. 5). The time-series suggest a gradual decrease in production of dissolved NH_4^+ in the sediment leading to decreasing concentrations with time. The pore water depth profiles of dissolved SO_4^{2-} show a decline with sediment depth at all time points. However, SO_4^{2-} concentrations remained relatively constant within the top 2 cm of surface sediment between day 12 and 33. Dissolved Fe^{2+}, Mn^{2+} and Ca^{2+} all show the development of distinct peaks in the pore water with time, and after 40 days those peaks disappear again. Pore water concentrations of HPO_4^{2-} generally increased with sediment depth for all time points, and concentrations within the top 2 cm were below the detection limit indicating removal. Dissolved H_4SiO_4 increased with sediment depth reaching concentration of up to 1 mM.

3.5. Diffusive Fluxes

Calculated diffusive fluxes of NH_4^+ into the oxic zone decreased during the incubation experiment from 4.7 to 1.8 mmol m^{-2} d^{-1} (Fig. 6A; Fig. S4; Table S3). Rates of SO_4^{2-} reduction estimated from the linear gradient of the decrease in pore water SO_4^{2-} in the surface sediment with depth generally also showed a decrease with time (Fig. 6B; Fig. S5; Table S3). The upward diffusive flux of Fe^{2+} greatly increased from day 5 to day 12 and then gradually decreased with time (Fig 6C; Fig. S6; Table S3). The upward diffusive flux of Mn showed an increase in the initial stage of the experiment and reached its maximum at day 18, followed by a decrease with time (Fig. 6D; Fig. S7; Table 3). The upward diffusive flux of Ca^{2+} showed no clear trend with time, however after 207 days the flux became extremely low (Fig. 6E; Fig. S8). The upward diffusive flux of H_4SiO_4 also showed an increase in the initial stage of the experiment, and reached its maximum at day 12, followed by a decrease with time (Fig. 6F; Fig. S9).

3.6. Solid-phase Profiles

The surface sediment in the oxic cores became more enriched in Fe oxides with time, with concentrations increasing from 53 to 485 μmol g^{-1} (Figure 7). The deeper sediment in the oxic cores and the entire anoxic control core had low or no Fe oxides. At day 5, FeS was strongly depleted

within the top 1 cm of the surface sediment and was gradually lost further with time. At day 621, most of the FeS within the top 2.5 cm of the surface sediment had been dissolved. The anoxic core did not show such a depletion of FeS in the surface sediment and even showed a slight increase in FeS. Solid-phase siderite remained rather constant with depth from day 5 to 33, but afterwards was gradually lost from the surface sediment. At day 621 a large proportion of the siderite was dissolved within the top 2 cm. Solid-phase siderite concentrations remained constant with depth in the anoxic control core. Solid-phase depth profiles of Mn oxides, metal bound P and metal oxide bound Si all showed a gradual increase in the surface sediment with time.

3.7. High-resolution Elemental Mapping

High-resolution desktop µXRF mapping of Fe, Mn, P and Ca of our core after 47 days of incubations revealed a subsurface sediment layer highly enriched in Fe and P (Fig. 8A). Subsurface enrichments in Fe, P and Mn in relatively thin layers were also observed in sediments populated by cable bacteria in the Gulf of Finland and Lake Grevelingen (Fig. 8B and C). In the latter system, the layers enriched in Fe, P, Mn broadened upon recolonization by macrofauna (Fig. 8D).

3. DISCUSSION

4.1. Metabolic Activity of Cable Bacteria

Cable bacteria in our incubation experiment demonstrated a rapid growth, since their abundance greatly increased after 5 days, and reached its peak at day 26 (Fig 1C). Such high abundances are similar to those observed in previous experiments, in which FeS-rich marine sediments from Aarhus Bay and Lake Grevelingen were incubated (Schauer et al. 2014; Burdorf et al. 2018). The activity of cable bacteria exerted a strong impact on the pore water depth profiles of pH, O_2, and $\sum H_2S$, as evident from the development of a pH maximum near the sediment-water interface, the strong pore water acidification in the deeper sediment and the development of a suboxic zone (Fig. 2A). These pore water depth profiles resemble the distinct biogeochemical fingerprint typical for active cable bacteria, as observed in previous laboratory incubation experiments (Risgaard-Petersen et al. 2012; Malkin et al. 2014; Schauer et al. 2014; Vasquez-Cardenas et al. 2015; Rao et al. 2016;

Burdorf et al. 2018). The widening of the suboxic zone with time (Fig 3) is a consequence of the downward expansion of the cable bacteria filament network (Schauer et al. 2014; Vasquez-Cardenas et al. 2015).

The EP depth profiles demonstrated that long-distance electron transport by cable bacteria was already active 5 days after the start of the experiment, as indicated by the increase of EP at depth to 0.4 mV). With time, the EP signal increased to higher values and also accumulated over a thicker depth horizon (Fig. 2B), indicating that cable bacteria activity both increased and extended to deeper sediment depth, which is also a consequence of the downward expansion of cable bacteria filaments. The EP reached a maximum after 18 days (1.3 mV; Fig. 2B) in concert with the highest current density of ~130 mmol e^- m^{-2} d^{-1} (Fig 4B). This maximum EP value and current density are similar in magnitude to those found in sediment incubations with seawater with a similar salinity (Damgaard et al. 2014). From day 18 onwards the EP and current density flux gradually decreased with time to 13 mmol e^- m^{-2} d^{-1} after 207 days (Fig. 4B), which implies a decrease in the metabolic activity of cable bacteria. The suboxic zone persisted long after the current density had decreased (Fig. 3).

To summarise, the metabolic activity of cable bacteria was likely highest between day 18 and day 26 based on the cable bacterial abundances, the extent of acidification of the pore water and the current density (Fig 1C; Fig 2A and Fig 4B).

4.2. Organic Matter Degradation

Ammonium fluxes are assumed to reflect rates of anaerobic degradation of organic matter (Fig. 5), and the observed decline during the experiment coincides with the decrease in activity of cable bacteria based on the EP profiles and current density (Fig. 2B; Fig 4B). This suggests that the availability of easily degradable organic matter plays a role in sustaining the metabolic activity of cable bacteria, most likely by controlling the rate of SO_4^{2-} reduction (Nielsen and Risgaard-Petersen 2015).

Rates of SO_4^{2-} reduction estimated from the linear gradient of the decrease in pore water SO_4^{2-} in the surface sediment with depth indeed also showed a decline during the experiment. We note,

however, that a direct measurement of SO_4^{2-} reduction rates (Fossing and Jørgensen 1989; Kallmeyer et al. 2004) would provide a better indicator, because SO_4^{2-} estimated from pore water profiles are in general lower than rates estimated from tracer experiments (Hermans et al. 2019a; Sandfeld et al. 2020). Another cause for a slight underestimation of our SO_4^{2-} reduction rates, is due to the effect of the electric field imposed by cable bacteria, which is not taken into account in Fick's law. Solutes can also move with respect to the fluid by electrostatic forces (Bockris and Reddy 1998). Given the relatively low strength of the electric field in the cores (<0.073V m^{-1} at day 18; as estimated from Fig. 2B), including the contribution of ionic drift to the sulphate flux would lead to SO_4^{2-} reduction rates that are at most 10-20% higher.

The metabolic activity of cable bacteria can lead to the production of SO_4^{2-} in the suboxic zone via anodic sulphide oxidation (Risgaard-Petersen et al. 2012; Rao et al. 2016). We suspect that this also explains the lack of change in pore water SO_4^{2-} with depth in the upper 2 cm of the sediment in our experiment between 12 and 40 days (Fig. 5). Despite relatively high SO_4^{2-} reduction rates ranging from 5.4 to 17.6 mmol m^{-2} d^{-1} (Fig. 6B; Table S3), pore water concentrations of ΣH_2S remained very low throughout the experiment (Fig. 2A). This is likely due to the direct consumption of ΣH_2S through the activity of cable bacteria, preventing ΣH_2S from accumulating in the pore water, or alternatively, precipitation of FeS by dissolved Fe^{2+} released from the dissolution of siderite.

Laboratory experiments have shown that S-oxidation by cable bacteria can play a dominant role in the O_2 uptake of coastal sediments (Nielsen et al. 2010; Schauer et al. 2014; Nielsen and Risgaard-Petersen 2015), and model analysis predicts up to 93% of the total O_2 uptake (Meysman et al. 2015). When we plot diffusive uptake of O_2 against the current density (i.e. upward flux of electrons towards the oxic zone), a linear relationship – with some scatter - emerges for days 12 to 621 (Fig. 9). However, the data points for day 0 and 5 during the initial stages of our experiment do not follow this linear relationship. We explain these findings as follows: At day 0, the cable bacteria were not active yet and other processes, such as aerobic respiration and oxidation of NH_4^+ and other solutes (Table 2) and solids (FeS) dominated the consumption of O_2. At day 5 and 12, the activity of cable bacteria and the oxidation of reduced products from anaerobic degradation of organic matter both contributed to

consumption of O_2. From day 12 onwards, both the O_2 consumption and electron flux follow a downward decrease with time (Fig. 9). If cable bacteria would account for all of the O_2 consumption, a ratio between the diffusive uptake of O_2 and the current density of 1:4 is expected (Fig. 1A; Nielsen et al. 2010). We find that from day 12 onwards, most data points plot rather close to the line for this 1:4 relationship (Fig. 9), suggesting that cathodic O_2 reduction by cable bacteria is responsible for nearly all O_2 consumption in the sediment (in line with the model results of Meysman et al. 2015). This however poses a problem for the nitrogen budget, because our data indicate complete removal of the NH_4^+ that diffuses upward into the oxic zone (Fig. 6A), and based on the solute fluxes, no escape to the overlying water (see section 2.4). This implies substantial O_2 consumption due to nitrification (Table 2). These findings can be explained, however, if we assume that at least part of the NO_3^- that is being formed near the sediment-water interface is also used for the metabolic activity of cable bacteria. It has been shown that cable bacteria can couple the oxidation of $\sum H_2S$ to NO_3^- in the absence of O_2 (Marzocchi et al. 2014). Our data suggest that this process may also occur in sediments where O_2 is present in concert with NO_3^- near the sediment-water interface. However, we cannot exclude release of NO_3^- to the water column or denitrification by other bacteria in the sediment. Another explanation is that cable bacteria might consume O_2 directly above the sediment-water interface, as recently has been proposed by Burdorf et al. (2018). Lastly, the current density might be slightly overestimated, since it ignores other sources that can create an electric potential, such as the diffusion potential (Revil et al. 2012; Nielsen and Risgaard-Petersen 2015).

4.3. Impact of Cable Bacteria on Fe, Mn and S Cycling

The activity of cable bacteria had a strong impact on the biogeochemistry of the surface sediment in our experiment (Fig. 7). Cable bacteria activity induced an intense acidification of the pore water in the suboxic zone (Fig 2A), which led to the dissolution of Fe and Mn minerals in deeper sediment layers, as can be inferred from the sharp maxima in dissolved Fe^{2+} and Mn^{2+} in the pore water reaching concentrations of up to ~1700 and ~80 µM, respectively (Fig. 5). The twenty-fold higher dissolved Fe^{2+} concentrations with respect to pore water Mn^{2+} can be attributed to the relatively higher availability of FeS and siderite compared to the availability of Mn carbonates in the sediment that was

used for incubation (Lenstra et al. 2020). The peaks in dissolved Fe^{2+} and Mn^{2+} in the pore water broadened over time spanning a depth of >5cm (Fig. 5; Fig. S6; Fig. S7).

The upward diffusive flux of dissolved Fe^{2+} and Mn^{2+} was highest after 12 days, reaching values of up to 3.16 and 0.16 mmol m^{-2} d^{-1} respectively. Fluxes subsequently gradually decreased with time (Fig. 6C and D). The continuous upward diffusion of dissolved Fe^{2+} and Mn^{2+} led to enrichments of poorly crystalline Fe and Mn oxides in the surface sediment (Fig. 7). Despite high upward fluxes of dissolved Fe^{2+} and Mn^{2+} towards the sediment-water interface, our solute flux incubations indicate there was little escape of Fe^{2+} and Mn^{2+} to the overlying water (see section 2.4). This implies that all Fe^{2+} and Mn^{2+} that diffused upward was precipitated as Fe and Mn oxides upon contact with O_2 or NO_3^- (Buresh and Moraghan 1976; Kuz'minskii et al. 1994; Straub et al. 1996). Little or no escape of dissolved Fe^{2+} from the sediment into the overlying water, was suggested previously for a field site with active cable bacteria based on diffusive flux calculations (Lake Grevelingen; Sulu-Gambari et al. 2016a) and was determined in flux incubations of cores during a laboratory experiment with cable bacteria (Rao et al. 2016).

At the start of the experiment, the sedimentary FeS content was (~25 µmol g^{-1}), which is not unusual for coastal sediments on the north-western Black Sea margin (Wijsman et al. 2001), but is low compared to sediments in eutrophic coastal systems (e.g. Morgan et al. 2012; Kraal et al. 2013; Hermans et al. 2019a). The solid-phase depth profiles reveal a gradual removal of the FeS in the surface sediment in our experiment over time (Fig. 7). At the end of our experiment (621 days), there was no longer any FeS within the top 1.5 cm of the sediment. While approximately 90 mmol m^{-2} of FeS was removed from the surface sediment within the first 5 days, a total of ~240 mmol m^{-2} was removed after 621 days (Fig. 10; Table 3). Likely, part of the FeS that was removed from the surface sediment within the first 5 days was removed through oxidation upon contact with O_2, rather than the metabolic activity of cable bacteria itself. The pore water acidification associated with cable bacteria activity led to a strong loss of siderite within the top 2 cm of the sediment, with a total removal of ~560 mmol m^{-2} during the experiment (Fig. 7; Fig. 10; Table 3). The depletion of sedimentary FeS

and siderite was directly proportional to the formation of Fe oxides near the sediment-water interface (Fig. 10), and accounted for 30% and 70% of the Fe oxides, respectively (Table 3).

With these data we cannot accurately determine the role of FeS versus SO_4^{2-} reduction in supplying the $\sum H_2S$ sustaining the activity of cable bacteria throughout the experiment. This is primarily related to the variability between cores, and for this type of calculation, the low temporal resolution of sampling. However, we can make an estimation of the relative role of SO_4^{2-} reduction and FeS dissolution in $\sum H_2S$ production, based on the pore water profiles of SO_4^{2-} and dissolved Fe^{2+}, and the solid-phase mass balance of FeS and siderite (Fig. 6B and C; Table 4). This estimation shows that SO_4^{2-} was mainly responsible for $\sum H_2S$ production, accounting for 85-99% (Table 4), and thus that the dissolution of FeS only played a minor role in providing $\sum H_2S$.

4.4. Impact of Cable Bacteria on Ca, P and Si Cycling

Cable bacteria activity is known to lead to dissolution of Ca carbonates, because of the strong acidification of the pore water (Risgaard-Petersen et al. 2012; Rao et al. 2016). We indeed find similar maxima in pore water Ca^{2+} during the experiment (Fig. 5) and a high upward flux of Ca^{2+} (up to ~18 mmol m^{-2} d^{-1}; Fig. 6E; Fig. S8) of which a substantial fraction (up to ~55%) escapes to the overlying water (Fig. S10; Table S4), which is consistent with a previous incubation experiment Rao et al. (2016).

Pore water depth profiles of HPO_4^{2-} reveal a production at depth and removal of all upward diffusing HPO_4^{2-} within the first 1-3 cm of the surface sediment (Fig. 5). A major proportion of this HPO_4^{2-} is bound to Fe oxides (Fig. 7). Given that a large proportion of the Fe oxides in our sediment cores derive from the dissolution of siderite, this suggests that the buffer mechanism that delays the benthic release of HPO_4^{2-} through retention of P associated with newly formed Fe oxides (Sulu-Gambari et al. 2016b), might also be active in systems that are relatively poor in sedimentary FeS.

The shape of the pore water HPO_4^{2-} profiles suggests that some of the HPO_4^{2-} is removed below the zone where Fe and Mn oxides are present (Fig. 5; Fig. 7). A possible explanation could be the formation of vivianite, an Fe(II) phosphate mineral. Vivianite formation in sediments typically occurs

when pore water levels of Fe^{2+} and HPO_4^{2-} are high and concentrations of ΣH_2S are low (Nriagu 1972), as observed in our study. In our experiment, free ΣH_2S does not accumulate in the pore water, which we attribute to removal through the activity of cable bacteria and FeS formation at depth (Fig. 2A; Fig. 7). Hence, cable bacteria may create a geochemical niche that allows the formation of vivianite in the suboxic zone. Further work with sediments with higher P concentrations would be needed to assess this with direct measurement techniques, such as X-ray spectroscopy (Egger et al. 2015; Kraal et al. 2017; Sulu-Gambari et al. 2018). Other sediment P pools, i.e. organic, authigenic and detrital P remained constant over time, indicating that the P contents determined for discrete sediment slices using sequential extractions were not affected by pore water acidification as a result of cable bacteria activity (Table S5).

Pore water H_4SiO_4 profiles show a typical increase with depth as observed upon dissolution of biogenic silica in marine sediments (Aller 2014). Fluxes of H_4SiO_4 towards the sediment-water interface range up to ~2.8 mmol m^{-2} d^{-1} and gradually decreased with time (Fig. 6F; Fig. S9). The results of the solute flux incubations indicate that most of this H_4SiO_4 escaped to the overlying water (ranging from 28 to 92%; Table S4; Fig. S10). The decline in the benthic release flux of H_4SiO_4 contrasts with results of a previous incubation experiment by Rao et al. (2016) with similar pore water concentrations of H_4SiO_4 reaching values up to ~1 mM. In their study, the flux remained constant over time, possibly because of differences in the amount of biogenic Si in the sediment. The solid-phase metal oxide bound Si pool in the surface sediment increased directly proportional to the formation of Fe oxides throughout the experiment (Fig. 7). Silica is known to absorb to Fe oxides (Sigg and Stumm 1981; Davis et al. 2002). Hence, the results suggest that the Fe oxides formed through the activity of cable bacteria captured some of the upward diffusing H_4SiO_4.

4.5. Sediment Marker for Cable Bacteria Activity

Visual observations of core photographs reveal the gradual development of an orange layer (oxic zone) up to 9 mm thick, overlying a grey layer (suboxic zone) and a black layer (sulphidic zone) during the experiment (Fig. S11). This colour zonation is typical for sediments that have been geochemically affected by cable bacteria activity, as seen both in laboratory experiments (Nielsen and

Risgaard-Petersen 2015) and at coastal field sites (Sulu-Gambari et al. 2016a). High-resolution elemental maps of our sediments reveal the development of a ~0.3 mm thin subsurface layer highly enriched in Fe oxides and associated P, 47 days after the start of the incubation (Fig. 8A). While the Fe oxide layer is clearly enriched in P, we also observed a second layer enriched in P very close to the sediment-water interface (Fig. 8A). This layer is located above the Fe oxide layer, and in this layer P is strongly correlated with Ca. Below, we describe the formation of this layer in more detail and explain why such subsurface enrichments, detected with µXRF, may act as an additional sediment marker for present or recent cable bacteria activity, also in cases where visual observations are not conclusive.

During the experiment, O_2 penetration varied within a narrow range and was initially fixed between 1 and 2 mm depth (Fig. 3A), with the layer highly enriched in Fe forming mostly at a depth of 2 mm (Fig. 8A). Such a range in O_2 penetration is in accordance with observations in coastal sediments (e.g. Seitaj et al. 2015). The formation of the Fe-enriched layer can be explained by rapid oxidation of upward diffusing Fe^{2+} upon contact with O_2 (and possibly NO_3^-; Fig. 6C). Directly, above the Fe oxide layer a broader ~0.8 mm thick Mn oxide layer was observed (Fig. 8A). This contrast in zonation between Fe and Mn is likely due to the slower oxidation kinetics of Mn^{2+} compared to Fe^{2+} (Burdige 1993; Luther 2010; Learman et al. 2011).

While the Fe oxide layer is clearly enriched in P, we also observed a second layer enriched in P close to the sediment-water interface (Fig. 8A). In this layer, P is strongly correlated with Ca. This layer likely consists of carbonate fluorapatite (CFA), a Ca-P mineral, which is typically formed in marine sediments (Van Cappellen and Berner 1988; Ruttenberg and Berner 1993). Possibly, the high pore water pH near the sediment-water interface (resulting from cathodic O_2 reduction by cable bacteria; Fig. 2A), promotes apatite formation (Bellier et al. 2006), and the elevated Ca^{2+} concentrations (Fig. 5) created a biogeochemical niche for the formation of CFA.

Such focusing of Fe, Mn, P and associated elements within a thin subsurface layer, as a consequence of cable bacteria activity, also occurs in the field. This was demonstrated by Hermans et

548 al. (Submitted) in a study of a coastal site in the Gulf of Finland where cable bacteria were recently
549 active. Here, µXRF mapping of resin embedded sediments revealed strong focusing of Fe oxides,
550 Mn(II) phosphates and Fe bound P within a 3 mm thick layer near the sediment-water interface (Fig.
551 8B). A re-assessment of the µXRF data of Sulu-Gambari et al. (2016a; 2018) of surface sediments
552 with active cable bacteria from seasonally hypoxic marine Lake Grevelingen in January also revealed
553 similar subsurface enrichments in Fe, Mn and P (Fig. 8C). Importantly, no visual signals for cable
554 bacteria based on the colour pattern of the sediment were observed at the time.

555 Macrofaunal activity likely counteracts or prevents strong focusing of Fe oxides and associated P
556 within such a thin subsurface layer at field sites. Bioturbation, i.e. mixing of the sediment, typically
557 leads to oxidation from the sediment surface downwards (Norkko et al. 2012). Bioirrigation can
558 efficiently pump O_2 into the pore water and thereby enhance the oxidation of dissolved Fe^{2+}
559 (Kristensen et al. 2012; Norkko et al. 2012), but is not expected to lead to such a sharp oxidation front
560 (Norkko et al. 2012; Hermans et al. 2019a). This is also evident from high-resolution elemental maps
561 of the surface sediment from Lake Grevelingen in May, which shows the disappearance of the thin
562 layer highly enriched in Fe and P formed by cable bacteria in January as a consequence of
563 macrofaunal activity in May (Fig. 8D; Seitaj et al. 2015; Sulu-Gambari et al. 2016b).

564 We conclude that the focusing of Fe, Mn and associated P within a thin layer below the sediment-
565 water interface is likely a consistent feature in sediments populated by active cable bacteria and may
566 act as an additional sediment marker for present or recent cable bacteria activity, both in laboratory
567 experiments and at field sites, also in cases where visual observations are not conclusive. Focussing of
568 Fe and Mn oxides in the surface sediment is not exclusively tied to the activity of cable bacteria, and
569 can also occur in the absence of cable bacteria. However, the upward fluxes of Fe^{2+} and Mn^{2+} in
570 sediments populated by cable bacteria, are higher due to active dissolution of Fe and Mn minerals at
571 depth (e.g. Risgaard-Petersen et al. 2012; Rao et al. 2016). Hence, within the same time frame
572 following an environmental perturbation (such as a transition to oxic bottom waters after a period of
573 anoxia or mixing of the sediment), more Fe^{2+} and Mn^{2+} can oxidise upon contact with O_2 near the
574 sediment-water interface and stronger enrichments of Fe and Mn minerals will be observed. Hence,

focusing of Fe and Mn oxides in subsurface sediments is likely more prominent and stronger in sediments populated by active cable bacteria compared to sediments where no cable bacteria are active under such conditions. Macrofaunal activity within natural environments likely counteracts or prevents strong focusing of Fe oxides and associated P within such a thin subsurface layer. When using standard techniques for sediment sampling (i.e. core slicing and chemical analysis of these slices), these layers may be missed due to the relatively coarse depth resolution. Hence, µXRF mapping of epoxy embedded sediment is recommended.

4.6. Cable Bacteria Activity at the Field Site

We can only speculate about the possible *in-situ* relevance of cable bacteria at the coastal site in the western Black Sea where the sediment for our incubation was collected. At this site, which is in a region that is subject to seasonal hypoxia (Capet et al. 2013), both bivalves (up to ~7200 ind. m^{-2}) and polychaetes (up to ~1700 ind. m^{-2}) were observed at the time of sampling (Lenstra et al. 2019). Macrofauna can inhibit the activity of cable bacteria through bioturbation by physically cutting and damaging the filaments, rendering them unable to transport electrons (Malkin et al. 2014). Recent work has shown, however, that in some cases, cable bacterial communities can also thrive in sediments with macrofauna (Burdorf et al. 2017; Malkin et al. 2017; Aller et al. 2019). In a study of bivalve reefs, cable bacteria were found to efficiently remove highly toxic ΣH_2S, which is beneficial for bivalves (Malkin et al. 2017). Cable bacteria can also be abundant in bioturbated deposits, when associated with stable subdomains of the bioturbated zone, such as worm tubes (Aller et al. 2019). In such settings, a more complex precipitation pattern, e.g. along tube linings is observed (Aller et al. 2019), than described here for laboratory experiments with defaunated sediments and field sediments with an impoverished macrofaunal population (Fig. 8A). Further field studies are required to assess the role of cable bacteria at our field site, preferably including an assessment of the burrow structures.

Conclusions

The results of our laboratory incubation (with a total duration of 621 days) show that cable bacteria can potentially strongly impact the Fe, Mn, P and S dynamics in coastal sediments. The strong acidity of the pore water associated with the activity of cable bacteria, which was monitored

using microsensor profiling of the EP during the experiment, led to dissolution of FeS and siderite and formation of Fe and Mn oxides and Ca-P in mineral form near the sediment surface. Our experimental results provide conclusive evidence for siderite dissolution driven by cable bacteria activity as a source of Fe that can form an Fe oxide-enriched surface layer. Both FeS and SO_4^{2-} reduction provided the $\sum H_2S$ required by cable bacteria to sustain their activity. Pore water $\sum H_2S$ was always low (<5 µM). Using µXRF mapping of epoxy embedded sediment, we show that the activity of cable bacteria led to the development of a thin subsurface sediment layer (0.3 mm) that was highly enriched in Fe and P. The position of this layer in the sediment was directly proportional to the O_2 penetration depth during the experiment. We show that a similar layer highly enriched in Fe and P was also formed in sediments of field locations populated by cable bacteria (i.e. marine Lake Grevelingen and the brackish Gulf of Finland). We suggest that such layers, which are not necessarily visible by eye, may be used as a marker of cable bacteria activity in sediments with low macrofaunal activity.

Acknowledgements. We are grateful to the captain and crew of R/V *Pelagia* for their support during the expedition (64PE411). We thank S. Hidalgo-Martinez for the FISH analysis and for the SEM image of the cable bacteria filaments. We thank F. Sulu-Gambari for sharing µXRF data for sediments from Lake Grevelingen. We also thank N. Geerlings, Z. Wang, K. Wunsch, T. Hakkert, W.K. Lenstra, N.A.G.M. van Helmond, P. Kraal, M. Egger, A. Tramper, T. Zalm and J.J. Mulder for analytical support.

Financial support. This research was funded by the Netherlands Organisation for Scientific Research (NWO), Vici Grant 865.13.005 to CPS. Further support was provided by Research Foundation Flanders FWO Grant G038819N, NWO Vici Grant 016.VICI.170.072 to FJRM and by the Danish National Research Foundation [Agreement nos. DNRF104 and DNRF136].

Review statement. This research was edited by Tina Treude and reviewed by two anonymous referees.

Code availability. All data, if not directly available from the tables and supplementary information, will be made available in the PANGAEA database. In the meantime data are available upon request to the main author.

Author contributions. MH and CPS designed the experiment. MH carried out the experiment and analysis. All authors interpreted the data. MH and CPS wrote the paper with comments provided by NRP and FJRM.

Competing interests. The authors declare that they have no conflict of interest.

References

Aller, R. 2014. Sedimentary diagenesis, depositional environments, and benthic fluxes.

Aller, R. C., J. Y. Aller, Q. Zhu, C. Heilbrun, I. Klingensmith, and A. Kaushik. 2019. Worm tubes as conduits for the electrogenic microbial grid in marine sediments. Science advances **5:** eaaw3651.

APHA. 2005. Standard methods for the examination of water and wastewater. American Public Health Association (APHA): Washington, DC, USA.

Atkinson, M. 1997. Elemental composition of commercial seasalts. Journal of Aquariculture and Aquatic Sciences **8:** 39-43.

Bellier, N., F. Chazarenc, and Y. Comeau. 2006. Phosphorus removal from wastewater by mineral apatite. Water research **40:** 2965-2971.

Berg, P., N. Risgaard-Petersen, and S. Rysgaard. 1998. Interpretation of measured concentration profiles in sediment pore water. Limnology and Oceanography **43:** 1500-1510.

Berner, R. A. 1980. Early diagenesis: a theoretical approach. Princeton University Press.

Bjerg, J. T., H. T. Boschker, S. Larsen, D. Berry, M. Schmid, D. Millo, P. Tataru, F. J. Meysman, M. Wagner, and L. P. Nielsen. 2018. Long-distance electron transport in individual, living cable bacteria. Proceedings of the National Academy of Sciences **115:** 5786-5791.

Bockris, J. O. M., and A. K. Reddy. 1998. Ion-ion interactions. Modern Electrochemistry 1: Ionics**:** 225-359.

Boudreau, B. P. 1997. Diagenetic models and their implementation. Springer Berlin.

Boyd, P., and M. Ellwood. 2010. The biogeochemical cycle of iron in the ocean. Nature Geoscience **3:** 675.

Breitburg, D., L. A. Levin, A. Oschlies, M. Grégoire, F. P. Chavez, D. J. Conley, V. Garçon, D. Gilbert, D. Gutiérrez, and K. Isensee. 2018. Declining oxygen in the global ocean and coastal waters. Science **359:** eaam7240.

Burdige, D. J. 1993. The biogeochemistry of manganese and iron reduction in marine sediments. Earth-Science Reviews **35:** 249-284.

Burdige, D. J. 2006. Geochemistry of marine sediments. Princeton University Press.

Burdorf, L. D., S. Y. Malkin, J. T. Bjerg, P. van Rijswijk, F. Criens, A. Tramper, and F. J. Meysman. 2018. The effect of oxygen availability on long-distance electron transport in marine sediments. Limnology and Oceanography **63:** 1799-1816.

Burdorf, L. D., A. Tramper, D. Seitaj, L. Meire, S. Hidalgo-Martinez, E.-M. Zetsche, H. T. Boschker, and F. J. Meysman. 2017. Long-distance electron transport occurs globally in marine sediments. Biogeosciences **14:** 683-701.

Buresh, R. J., and J. Moraghan. 1976. Chemical Reduction of Nitrate by Ferrous Iron 1. Journal of Environmental Quality **5:** 320-325.

669 Burton, E. D., R. T. Bush, and L. A. Sullivan. 2006. Fractionation and extractability of sulfur, iron
670 and trace elements in sulfidic sediments. Chemosphere **64:** 1421-1428.
671 Burton, E. D., L. A. Sullivan, R. T. Bush, S. G. Johnston, and A. F. Keene. 2008. A simple and
672 inexpensive chromium-reducible sulfur method for acid-sulfate soils. Applied Geochemistry
673 **23:** 2759-2766.
674 Capet, A., J.-M. Beckers, and M. Grégoire. 2013. Drivers, mechanisms and long-term variability of
675 seasonal hypoxia on the Black Sea northwestern shelf–is there any recovery after
676 eutrophication. Biogeosciences **10:** 3943-3962.
677 Claff, S. R., L. A. Sullivan, E. D. Burton, and R. T. Bush. 2010. A sequential extraction procedure for
678 acid sulfate soils: partitioning of iron. Geoderma **155:** 224-230.
679 Cornelissen, R., A. Bøggild, R. Thiruvallur Eachambadi, R. I. Koning, A. Kremer, S. Hidalgo-
680 Martinez, E.-M. Zetsche, L. R. Damgaard, R. Bonné, and J. Drijkoningen. 2018. The cell
681 envelope structure of cable bacteria. Frontiers in microbiology **9:** 3044.
682 Coull, B. C., and G. T. Chandler. 2001. Meiobenthos*, p. 726-731. *In* J. H. Steele [ed.]. Academic
683 Press.
684 Damgaard, L. R., N. Risgaard-Petersen, and L. P. Nielsen. 2014. Electric potential microelectrode for
685 studies of electrobiogeophysics. Journal of Geophysical Research: Biogeosciences **119:** 1906-
686 1917.
687 Davis, C. C., H.-W. Chen, and M. Edwards. 2002. Modeling silica sorption to iron hydroxide.
688 Environmental science & technology **36:** 582-587.
689 Diaz, R. J., and R. Rosenberg. 2008. Spreading dead zones and consequences for marine ecosystems.
690 science **321:** 926-929.
691 Egger, M., T. Jilbert, T. Behrends, C. Rivard, and C. P. Slomp. 2015. Vivianite is a major sink for
692 phosphorus in methanogenic coastal surface sediments. Geochimica et Cosmochimica Acta
693 **169:** 217-235.
694 Fofonoff, N. P., and R. Millard Jr. 1983. Algorithms for the computation of fundamental properties of
695 seawater.
696 Fossing, H., and B. B. Jørgensen. 1989. Measurement of bacterial sulfate reduction in sediments:
697 evaluation of a single-step chromium reduction method. Biogeochemistry **8:** 205-222.
698 Geerlings, N., E.-M. Zetsche, S. Hidalgo-Martinez, J. J. Middelburg, and F. J. Meysman. 2019.
699 Mineral formation induced by cable bacteria performing long-distance electron transport in
700 marine sediments. Biogeosciences **16:** 811-829.
701 Glud, R. N. 2008. Oxygen dynamics of marine sediments. Marine Biology Research **4:** 243-289.
702 Hermans, M., M. Astudillo Pascual, T. Behrends, W. K. Lenstra, D. J. Conley, and C. P. Slomp.
703 Submitted. Coupled dynamics of iron, manganese and phosphorus in brackish coastal
704 sediments populated by cable bacteria.
705 Hermans, M., W. Lenstra, S. Hidalgo-Martinez, N. A. van Helmond, R. Witbaard, F. Meysman, S.
706 Gonzalez, and C. P. Slomp. 2019a. Abundance and Biogeochemical Impact of Cable Bacteria
707 in Baltic Sea Sediments. Environmental science & technology **53:** 7494-7503.
708 Hermans, M., W. K. Lenstra, N. A. van Helmond, T. Behrends, M. Egger, M. J. Séguret, E.
709 Gustafsson, B. G. Gustafsson, and C. P. Slomp. 2019b. Impact of natural re-oxygenation on
710 the sediment dynamics of manganese, iron and phosphorus in a euxinic Baltic Sea basin.
711 Geochimica et Cosmochimica Acta **246:** 174-196.
712 Hovanec, T. A., and J. L. Coshland. 2004. A chemical analysis of select trace elements in synthetic
713 sea salts and natural seawater. Sea Scope, Aquarium Systems **21**.
714 Jeroschewski, P., C. Steuckart, and M. Kühl. 1996. An amperometric microsensor for the
715 determination of H2S in aquatic environments. Analytical Chemistry **68:** 4351-4357.
716 Jilbert, T., G. de Lange, and G. J. Reichart. 2008. Fluid displacive resin embedding of laminated
717 sediments: preserving trace metals for high-resolution paleoclimate investigations. Limnology
718 and Oceanography: Methods **6:** 16-22.
719 Jilbert, T., and C. P. Slomp. 2013. Iron and manganese shuttles control the formation of authigenic
720 phosphorus minerals in the euxinic basins of the Baltic Sea. Geochimica et Cosmochimica
721 Acta **107:** 155-169.

Kallmeyer, J., T. G. Ferdelman, A. Weber, H. Fossing, and B. B. Jørgensen. 2004. A cold chromium distillation procedure for radiolabeled sulfide applied to sulfate reduction measurements. Limnology and Oceanography: Methods **2:** 171-180.

Kemp, W., J. Testa, D. Conley, D. Gilbert, and J. Hagy. 2009. Temporal responses of coastal hypoxia to nutrient loading and physical controls. Biogeosciences **6:** 2985-3008.

Kjeldsen, K. U., L. Schreiber, C. A. Thorup, T. Boesen, J. T. Bjerg, T. Yang, M. S. Dueholm, S. Larsen, N. Risgaard-Petersen, and M. Nierychlo. 2019. On the evolution and physiology of cable bacteria. Proceedings of the National Academy of Sciences **116:** 19116-19125.

Koroleff, F. 1969. Determination of ammonia as indophenol blue. International Council for the Exploration of the Sea (ICES) **9**.

Kraal, P., E. D. Burton, and R. T. Bush. 2013. Iron monosulfide accumulation and pyrite formation in eutrophic estuarine sediments. Geochimica et Cosmochimica Acta **122:** 75-88.

Kraal, P., N. Dijkstra, T. Behrends, and C. P. Slomp. 2017. Phosphorus burial in sediments of the sulfidic deep Black Sea: Key roles for adsorption by calcium carbonate and apatite authigenesis. Geochimica et Cosmochimica Acta **204:** 140-158.

Kraal, P., and C. P. Slomp. 2014. Rapid and extensive alteration of phosphorus speciation during oxic storage of wet sediment samples. PloS one **9:** e96859.

Kraal, P., C. P. Slomp, A. Forster, M. M. Kuypers, and A. Sluijs. 2009. Pyrite oxidation during sample storage determines phosphorus fractionation in carbonate-poor anoxic sediments. Geochimica et Cosmochimica Acta **73:** 3277-3290.

Kristensen, E., K. D. Kristiansen, and M. H. Jensen. 2003. Temporal behavior of manganese and iron in a sandy coastal sediment exposed to water column anoxia. Estuaries **26:** 690-699.

Kristensen, E., G. Penha-Lopes, M. Delefosse, T. Valdemarsen, C. O. Quintana, and G. T. Banta. 2012. What is bioturbation? The need for a precise definition for fauna in aquatic sciences. Marine Ecology Progress Series **446:** 285-302.

Kristiansen, K., E. Kristensen, and E. Jensen. 2002. The influence of water column hypoxia on the behaviour of manganese and iron in sandy coastal marine sediment. Estuarine, Coastal and Shelf Science **55:** 645-654.

Kuz'minskii, Y. V., A. Andriiko, and L. Nyrkova. 1994. Chemical and phase composition of manganese oxides obtained by Mn (II) oxidation in nitrate solutions. Journal of power sources **52:** 49-53.

Larsen, S., L. P. Nielsen, and A. Schramm. 2015. Cable bacteria associated with long-distance electron transport in New England salt marsh sediment. Environmental microbiology reports **7:** 175-179.

Learman, D., B. Voelker, A. Vazquez-Rodriguez, and C. Hansel. 2011. Formation of manganese oxides by bacterially generated superoxide. Nature Geoscience **4:** 95.

Lenstra, W., M. Hermans, M. Séguret, R. Witbaard, T. Behrends, N. Dijkstra, N. Van Helmond, P. Kraal, P. Laan, and M. Rijkenberg. 2019. The shelf-to-basin iron shuttle in the Black Sea revisited. Chemical Geology **511:** 314-341.

Lenstra, W., M. Séguret, T. Behrends, R. Groeneveld, M. Hermans, R. Witbaard, and C. Slomp. 2020. Controls on the shuttling of manganese over the northwestern Black Sea shelf and its fate in the euxinic deep basin. Geochimica et Cosmochimica Acta **273:** 177-204.

Luther, G. W. 2010. The role of one-and two-electron transfer reactions in forming thermodynamically unstable intermediates as barriers in multi-electron redox reactions. Aquatic Geochemistry **16:** 395-420.

Madison, A. S., B. M. Tebo, A. Mucci, B. Sundby, and G. W. Luther. 2013. Abundant porewater Mn (III) is a major component of the sedimentary redox system. science **341:** 875-878.

Malkin, S. Y., A. M. Rao, D. Seitaj, D. Vasquez-Cardenas, E.-M. Zetsche, S. Hidalgo-Martinez, H. T. Boschker, and F. J. Meysman. 2014. Natural occurrence of microbial sulphur oxidation by long-range electron transport in the seafloor. The ISME journal **8:** 1843-1854.

Malkin, S. Y., D. Seitaj, L. D. Burdorf, S. Nieuwhof, S. Hidalgo-Martinez, A. Tramper, N. Geeraert, H. De Stigter, and F. J. Meysman. 2017. Electrogenic sulfur oxidation by cable bacteria in bivalve reef sediments. Frontiers in Marine Science **4:** 28.

Marzocchi, U., D. Trojan, S. Larsen, R. L. Meyer, N. P. Revsbech, A. Schramm, L. P. Nielsen, and N. Risgaard-Petersen. 2014. Electric coupling between distant nitrate reduction and sulfide oxidation in marine sediment. The ISME journal **8:** 1682-1690.

Meysman, F. J. 2018. Cable bacteria take a new breath using long-distance electricity. Trends in microbiology **26:** 411-422.

Meysman, F. J., R. Cornelissen, S. Trashin, R. Bonné, S. H. Martinez, J. van der Veen, C. J. Blom, C. Karman, J.-L. Hou, and R. T. Eachambadi. 2019. A highly conductive fibre network enables centimetre-scale electron transport in multicellular cable bacteria. Nature communications **10:** 1-8.

Meysman, F. J., N. Risgaard-Petersen, S. Y. Malkin, and L. P. Nielsen. 2015. The geochemical fingerprint of microbial long-distance electron transport in the seafloor. Geochimica et Cosmochimica Acta **152:** 122-142.

Millero, F. J., T. Plese, and M. Fernandez. 1988. The dissociation of hydrogen sulfide in seawater 1. Limnology and Oceanography **33:** 269-274.

Morgan, B., E. D. Burton, and A. W. Rate. 2012. Iron monosulfide enrichment and the presence of organosulfur in eutrophic estuarine sediments. Chemical Geology **296:** 119-130.

Müller, H., J. Bosch, C. Griebler, L. R. Damgaard, L. P. Nielsen, T. Lueders, and R. U. Meckenstock. 2016. Long-distance electron transfer by cable bacteria in aquifer sediments. The ISME journal **10:** 2010-2019.

Murphy, J., and J. Riley. 1958. A single-solution method for the determination of soluble phosphate in sea water. Journal of the Marine Biological Association of the United Kingdom **37:** 9-14.

Naudet, V., and A. Revil. 2005. A sandbox experiment to investigate bacteria-mediated redox processes on self-potential signals. Geophysical Research Letters **32**.

Nielsen, L. P., and N. Risgaard-Petersen. 2015. Rethinking sediment biogeochemistry after the discovery of electric currents. Annual review of marine science **7:** 425-442.

Nielsen, L. P., N. Risgaard-Petersen, H. Fossing, P. B. Christensen, and M. Sayama. 2010. Electric currents couple spatially separated biogeochemical processes in marine sediment. Nature **463:** 1071-1074.

Norkko, J., D. C. Reed, K. Timmermann, A. Norkko, B. G. Gustafsson, E. Bonsdorff, C. P. Slomp, J. Carstensen, and D. J. Conley. 2012. A welcome can of worms? Hypoxia mitigation by an invasive species. Global Change Biology **18:** 422-434.

Nriagu, J. O. 1972. Stability of vivianite and ion-pair formation in the system fe3 (PO4) 2-H3PO4H3PO4-H2o. Geochimica et Cosmochimica Acta **36:** 459-470.

Pernthaler, J., F.-O. Glöckner, W. Schönhuber, and R. Amann. 2001. Fluorescence in situ hybridization (FISH) with rRNA-targeted oligonucleotide probes. Methods in microbiology **30:** 207-226.

Pfeffer, C., S. Larsen, J. Song, M. Dong, F. Besenbacher, R. L. Meyer, K. U. Kjeldsen, L. Schreiber, Y. A. Gorby, and M. Y. El-Naggar. 2012. Filamentous bacteria transport electrons over centimetre distances. Nature **491:** 218-221.

Poulton, S. W., and D. E. Canfield. 2005. Development of a sequential extraction procedure for iron: implications for iron partitioning in continentally derived particulates. Chemical Geology **214:** 209-221.

Rabalais, N. N., W.-J. Cai, J. Carstensen, D. J. Conley, B. Fry, X. Hu, Z. Quinones-Rivera, R. Rosenberg, C. P. Slomp, and R. E. Turner. 2014. Eutrophication-driven deoxygenation in the coastal ocean. Oceanography **27:** 172-183.

Rabalais, N. N., R. E. Turner, and W. J. Wiseman Jr. 2002. Gulf of Mexico hypoxia, aka "The dead zone". Annual Review of ecology and Systematics **33:** 235-263.

Rabouille, C., L. Denis, K. Dedieu, G. Stora, B. Lansard, and C. Grenz. 2003. Oxygen demand in coastal marine sediments: comparing in situ microelectrodes and laboratory core incubations. Journal of Experimental Marine Biology and Ecology **285:** 49-69.

Raiswell, R., and D. E. Canfield. 2012. The iron biogeochemical cycle past and present. Geochemical perspectives **1:** 1-2.

Rao, A. M., S. Y. Malkin, S. Hidalgo-Martinez, and F. J. Meysman. 2016. The impact of electrogenic sulfide oxidation on elemental cycling and solute fluxes in coastal sediment. Geochimica et Cosmochimica Acta **172:** 265-286.

Rasmussen, H., and B. B. Jørgensen. 1992. Microelectrode studies of seasonal oxygen uptake in a coastal sediment: role of molecular diffusion. Marine ecology progress series. Oldendorf **81:** 289-303.

Reed, D. C., C. P. Slomp, and B. G. Gustafsson. 2011. Sedimentary phosphorus dynamics and the evolution of bottom-water hypoxia: A coupled benthic–pelagic model of a coastal system. Limnology and Oceanography **56:** 1075-1092.

Revil, A., M. Karaoulis, T. Johnson, and A. Kemna. 2012. Some low-frequency electrical methods for subsurface characterization and monitoring in hydrogeology. Hydrogeology Journal **20:** 617-658.

Revil, A., C. Mendonça, E. Atekwana, B. Kulessa, S. Hubbard, and K. Bohlen. 2010. Understanding biogeobatteries: Where geophysics meets microbiology. Journal of Geophysical Research: Biogeosciences **115**.

Riedel, B., M. Zuschin, and M. Stachowitsch. 2012. Tolerance of benthic macrofauna to hypoxia and anoxia in shallow coastal seas: a realistic scenario. Marine Ecology Progress Series **458:** 39-52.

Risgaard-Petersen, N., M. Kristiansen, R. B. Frederiksen, A. L. Dittmer, J. T. Bjerg, D. Trojan, L. Schreiber, L. R. Damgaard, A. Schramm, and L. P. Nielsen. 2015. Cable bacteria in freshwater sediments. Applied and environmental microbiology **81:** 6003-6011.

Risgaard-Petersen, N., A. Revil, P. Meister, and L. P. Nielsen. 2012. Sulfur, iron-, and calcium cycling associated with natural electric currents running through marine sediment. Geochimica et Cosmochimica Acta **92:** 1-13.

Risgaard-Petersen, N., L. R. Damgaard, A. Revil, and L. P. Nielsen. 2014. Mapping electron sources and sinks in a marine biogeobattery. Journal of Geophysical Research: Biogeosciences **119:** 1475-1486.

Ruttenberg, K. C. 1992. Development of a sequential extraction method for different forms of phosphorus in marine sediments. Limnology and oceanography **37:** 1460-1482.

Ruttenberg, K. C., and R. A. Berner. 1993. Authigenic apatite formation and burial in sediments from non-upwelling, continental margin environments. Geochimica et cosmochimica acta **57:** 991-1007.

Sandfeld, T., U. Marzocchi, C. Petro, A. Schramm, and N. Risgaard-Petersen. 2020. Electrogenic sulfide oxidation mediated by cable bacteria stimulates sulfate reduction in freshwater sediments. The ISME Journal **14:** 1233-1246.

Schauer, R., N. Risgaard-Petersen, K. U. Kjeldsen, J. J. T. Bjerg, B. B. Jørgensen, A. Schramm, and L. P. Nielsen. 2014. Succession of cable bacteria and electric currents in marine sediment. The ISME journal **8:** 1314.

Schmidtko, S., L. Stramma, and M. Visbeck. 2017. Decline in global oceanic oxygen content during the past five decades. Nature **542:** 335.

Seitaj, D., R. Schauer, F. Sulu-Gambari, S. Hidalgo-Martinez, S. Y. Malkin, L. D. Burdorf, C. P. Slomp, and F. J. Meysman. 2015. Cable bacteria generate a firewall against euxinia in seasonally hypoxic basins. Proceedings of the National Academy of Sciences **112:** 13278-13283.

Sigg, L., and W. Stumm. 1981. The interaction of anions and weak acids with the hydrous goethite (α-FeOOH) surface. Colloids and surfaces **2:** 101-117.

Slomp, C. P., E. H. Epping, W. Helder, and W. V. Raaphorst. 1996. A key role for iron-bound phosphorus in authigenic apatite formation in North Atlantic continental platform sediments. Journal of Marine Research **54:** 1179-1205.

Soetaert, K., T. Petzoldt, and F. Meysman. 2010. Marelac: Tools for aquatic sciences. R package version.

Straub, K. L., M. Benz, B. Schink, and F. Widdel. 1996. Anaerobic, nitrate-dependent microbial oxidation of ferrous iron. Appl. Environ. Microbiol. **62:** 1458-1460.

Sulu-Gambari, F., M. Hagens, T. Behrends, D. Seitaj, F. J. Meysman, J. Middelburg, and C. P. Slomp. 2018. Phosphorus cycling and burial in sediments of a seasonally hypoxic Marine Basin. Estuaries and Coasts **41:** 921-939.

Sulu-Gambari, F., D. Seitaj, T. Behrends, D. Banerjee, F. J. Meysman, and C. P. Slomp. 2016a. Impact of cable bacteria on sedimentary iron and manganese dynamics in a seasonally-hypoxic marine basin. Geochimica et Cosmochimica Acta **192:** 49-69.

Sulu-Gambari, F., D. Seitaj, F. J. Meysman, R. Schauer, L. Polerecky, and C. P. Slomp. 2016b. Cable bacteria control iron–phosphorus dynamics in sediments of a coastal hypoxic basin. Environmental science & technology **50:** 1227-1233.

Trojan, D., L. Schreiber, J. T. Bjerg, A. Bøggild, T. Yang, K. U. Kjeldsen, and A. Schramm. 2016. A taxonomic framework for cable bacteria and proposal of the candidate genera Electrothrix and Electronema. Systematic and applied microbiology **39:** 297-306.

Van Cappellen, P., and R. A. Berner. 1988. A mathematical model for the early diagenesis of phosphorus and fluorine in marine sediments; apatite precipitation. American Journal of Science **288:** 289-333.

van de Velde, S., L. Lesven, L. D. Burdorf, S. Hidalgo-Martinez, J. S. Geelhoed, P. Van Rijswijk, Y. Gao, and F. J. Meysman. 2016. The impact of electrogenic sulfur oxidation on the biogeochemistry of coastal sediments: A field study. Geochimica et Cosmochimica Acta **194:** 211-232.

Vasquez-Cardenas, D., J. Van De Vossenberg, L. Polerecky, S. Y. Malkin, R. Schauer, S. Hidalgo-Martinez, V. Confurius, J. J. Middelburg, F. J. Meysman, and H. T. Boschker. 2015. Microbial carbon metabolism associated with electrogenic sulphur oxidation in coastal sediments. The ISME journal **9:** 1966.

Wang, Y., and P. Van Cappellen. 1996. A multicomponent reactive transport model of early diagenesis: Application to redox cycling in coastal marine sediments. Geochimica et Cosmochimica Acta **60:** 2993-3014.

Wijsman, J. W., J. J. Middelburg, P. M. Herman, M. E. Böttcher, and C. H. Heip. 2001. Sulfur and iron speciation in surface sediments along the northwestern margin of the Black Sea. Marine Chemistry **74:** 261-278.

TABLES AND FIGURES

Table 1. Key site characteristics: latitude, longitude, water depth, bottom water O_2 concentration, *in-situ* O_2 uptake, *in-situ* O_2 penetration depth in the sediment, porosity and salinity. These data were retrieved from Lenstra et al. (2019). Our study site is station 9 in Lenstra et al. (2019).

Black Sea (Station 9)		**Unit**
Latitude	44°34.9’	N
Longitude	29°11.4’	E
Water depth	27	m
Bottom water O_2	92	µM
O_2 uptake	25.8 ± 1.77	mmol m^{-2} d^{-1}
O_2 penetration depth	2.25	mm
Porosity	0.86	-
Salinity	17.881	-
Avg. organic carbon content (0-0.5 cm)	1.8%	

Table 2. Mass balance of O_2 consumption. The diffusive uptake of O_2 as calculated from the O_2 depth profiles (column 1) was compared to the potential O_2 demand from the oxidation of NH_4^+, Fe^{2+} and Mn^{2+} (column 2-4). The O_2 consumption of the oxidation of NH_4^+, Fe^{2+} and Mn^{2+} was determined based on the stoichiometry of NH_4^+, Fe^{2+} and Mn^{2+} oxidation with O_2 as described in Reed et al. (2011). The oxidation of dissolved Fe^{2+} and Mn^{2+} only played a minor role in the total O_2 consumption during the experiment, contributing only 0.9 to 3.8% and 0.1 to 0.4%, respectively.

		Potential O_2 Demand			
	O_2 [mmol m^{-2} d^{-1}]	**NH_4^+ [mmol m^{-2} d^{-1}]**	**Fe^{2+} [mmol m^{-2} d^{-1}]**	**Mn^{2+} [mmol m^{-2} d^{-1}]**	**e^- [mmol m^{-2} d^{-1}]**
Day 5	-23.35	9.42	0.21	0.05	82.68
Day 12	-23.24	8.46	0.89	0.09	111.94
Day 18	-21.10	8.04	0.70	0.08	127.97
Day 26	-23.00	7.58	0.63	0.07	97.55
Day 33	-22.80	5.06	0.62	0.05	84.16
Day 40	-19.60	4.88	0.60	0.06	76.31
Day 207	-6.90	3.52	0.08	0.01	13.10
Day 621	-3.25	N/A	0.03	0.01	9.47

Table 3. Mass balance of Fe. Time-series of the depth integrated (0-5 cm) increase in Fe oxides and the depth integrated (0-5 cm) depletion of FeS and $FeCO_3$ (siderite) in mmol m^{-2}. All values are reported in mmol Fe m^{-2}. Negative values represent a decrease, whereas positive values indicate an increase in the mineral pools.

	ΔFe oxides [mmol m^{-2}]	**ΔFeS [mmol m^{-2}]**	**$\Delta FeCO_3$ [mmol m^{-2}]**
Day 5	120	-90	-42
Day 12	170	-90	-126
Day 18	189	-105	-92
Day 26	276	-174	-99
Day 33	315	-176	-109
Day 40	412	-223	-200
Day 207	523	-236	-341
Day 621	874	-242	-566

Table 4. Sources of $\sum H_2S$ calculated from the reduction of SO_4^{2-} and the dissolution of FeS. The numbers are presented either as mmol m^{-2} d^{-1} or as the relative percentage of the $\sum H_2S$ production. The amount of S from the dissolution of FeS was estimated from the upward diffusive flux of Fe^{2+} (Fig. 6C) and the relative fraction of FeS (FeS/FeS+siderite) based on the mass balance calculations (Table 3).

	S from SO_4^{2-} reduction [mmol m^{-2} d^{-1}]	**S from FeS dissolution [mmol m^{-2} d^{-1}]**	**S from SO_4^{2-} reduction [%]**	**S from FeS dissolution [%]**
Day 5	10.49	0.56	95%	5%
Day 12	17.60	1.48	92%	8%
Day 18	8.87	1.50	86%	14%
Day 26	11.15	1.61	87%	13%
Day 33	8.54	1.52	85%	15%
Day 40	7.57	1.25	86%	14%
Day 207	10.38	0.13	99%	1%
Day 621	5.36	0.03	99%	1%

Fig. 1. (A) Geochemical pore water fingerprint typical for cable bacteria activity. This fingerprint is defined by a distinct pH profile (light grey line) and a sub-oxic zone that is devoid of O_2 (red line) and H_2S (blue line). The cable bacteria filaments are depicted in yellow. On the background, the sediment core photograph, taken 278 days after the start of the experiment, shows a distinct colour zonation where (1) the oxic zone displays an orange colour (2) the suboxic zone has a grey colour and (3) the sulphidic zone has a black colour. The scale bar denotes a distance of 6 cm, with 0.5 cm intervals. **(B)** Bathymetric map of the Black Sea. The purple star indicates the location of our study site (44°34.93`N, 29°11.38`E), which was sampled with R/V *Pelagia* in September 2015. Further details are provided in Lenstra et al. (2019). **(C)** Volumetric density of cable bacteria [m cm^{-3}] in the top 2.5 cm of the sediment, for *in-situ* as well as for three time points during the incubation experiment **(D)** SEM image of a cable bacteria filament that was extracted from the surface sediment after 40 days.

Fig. 2. (A) Time-series of the pore water pH (black), O_2 (red) and $\sum H_2S$ (blue) signatures of the incubated sediment. (**B)** Development of the EP depth profile in the incubated sediment over time. The dashed-line at 0 mm depth represents the sediment-water interface. The blue boxes indicate the overlying water, whereas the underlying light grey boxes represent the sediment. The EP depth profiles represent an average of 3 replicate measurements. The error bars indicate the minimum and maximum EP values that were observed. The orange depth profiles represent duplicate measurement performed on a different core.

Fig. 3. Time-series of the development of the oxic zone (orange), suboxic zone (light grey) and the anoxic/sulphidic zone (dark grey) in the sediment. These zones were calculated from 3 replicate microelectrode depth profiles retrieved from two different cores.

Fig. 4. Time-series of the **(A)** diffusive O_2 uptake in mmol O_2 m^{-2} d^{-1} and **(B)** current density as a consequence of long-distance electron transport (e^-) in mmol e^- m^{-2} d^{-1} in the sediment incubation.

Fig. 5. Time-series of pore water depth profiles of NH_4^+ (orange), SO_4^{2-} (purple), Fe^{2+} (red), Mn^{2+} (green), Ca^{2+} (grey), HPO_4^{2-} (blue) and H_4SiO_4 (yellow). The control core was sampled at day 621.

Fig. 6. Time-series of diffusive fluxes calculated from the linear gradient of the pore water profiles of **(A)** NH_4^+, **(B)** SO_4^{2-}, **(C)** Fe^{2+}, **(D)** Mn^{2+}, **(E)** Ca^{2+} and **(F)** H_4SiO_4 in mmol m^{-2} d^{-1} towards the oxic zone of the sediment, based on the linear pore water gradients (Section 1.6; Fig. S3-S4). Here, a positive value indicates an upward flux, whereas a negative value represents a downward flux. N/A = not available. The control core was sampled at day 621.

963 **Fig. 7.** Time-series of solid-phase depth profiles of Fe oxides (red), FeS (black), siderite (grey), Mn oxides (green), metal
964 bound P (blue) and metal oxide bound Si (yellow).
965
966 **Fig. 8.** High-resolution elemental maps of Fe (red), Mn (green), P (blue) and Ca (white) of surface sediments. These maps
967 are shown in true vertical orientation and the colours accentuate the relative count intensities adjusted for brightness and
968 contrast to highlight the features in the sediment. The tick marks represent 1 mm intervals. µXRF maps of the surface
969 sediment **(A)** from the incubation experiment, **(B)** from the Gulf of Finland at site GOF5 in June (Hermans et al. Submitted),
970 **(C)** from Lake Grevelingen in January (when cable bacteria become active) and **(D)** from Lake Grevelingen in May
971 (showing the effects of bioturbation as described in Seitaj et al. (2015)).
972
973 **Fig. 9.** The relationship between the diffusive uptake of O_2 (mmol O_2 m^{-2} d^{-1}) and the current density of long-distance
974 electron transport (mmol e^- m^{-2} d^{-1}). Red triangles are data for days 0 and 5. Green diamonds are data for all other time
975 points. The blue line represents the expected correlation between the cathodic O_2 consumption rate and the current density
976 assuming a 1:4 ratio (Nielsen et al. 2010). Here, a positive value indicates an upward flux, whereas a negative value
977 represents a downward flux.
978
979 **Fig. 10.** Time-series of the depth integrated (0-5 cm) increase in Fe oxides (red) and the depletion of FeS (black) and siderite
980 (grey) in mmol m^{-2}. Negative values represent a decrease, whereas positive values indicate an increase in the mineral pools.

A

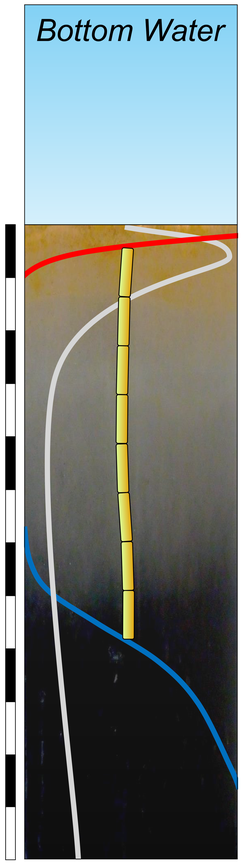

O_2

pH

H_2S

Cable Bacteria

Reduction: $O_2 + 4\ e^- + 4\ H^+ \rightarrow H_2O$

Oxidation: $H_2S + 4\ H_2O \rightarrow SO_4^{2-} + 10\ H^+ + 8\ e^-$

B

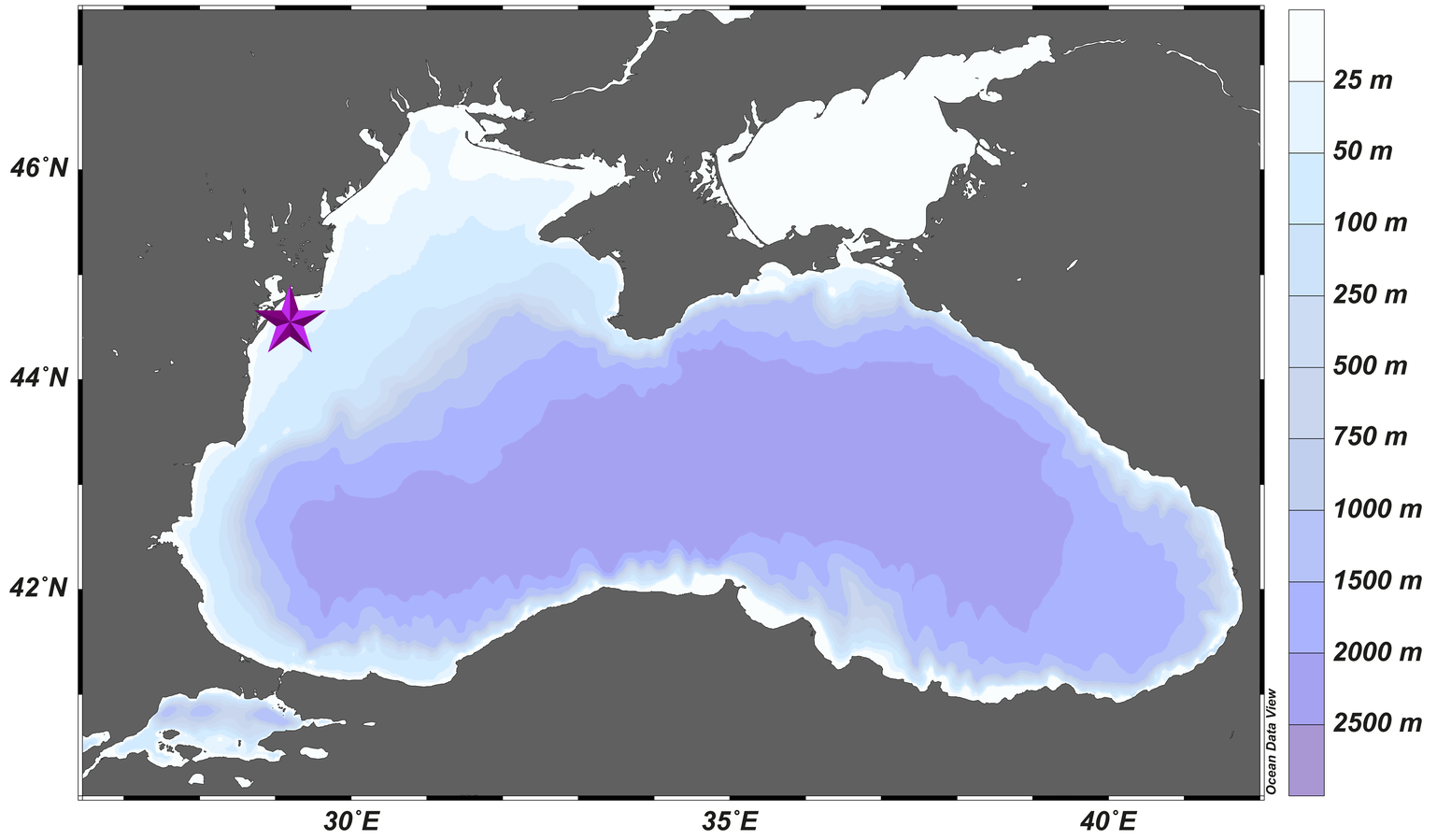

C

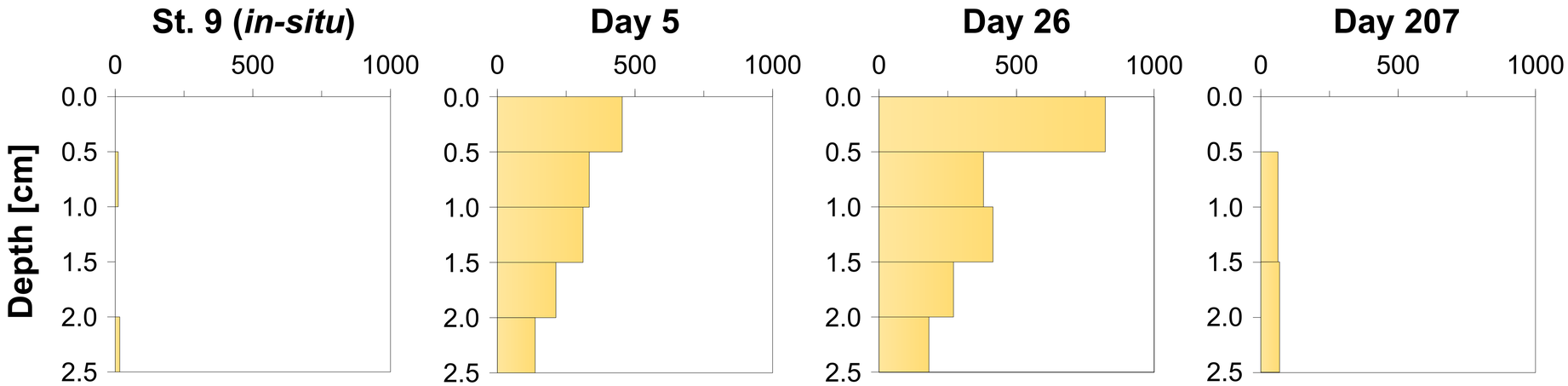

D

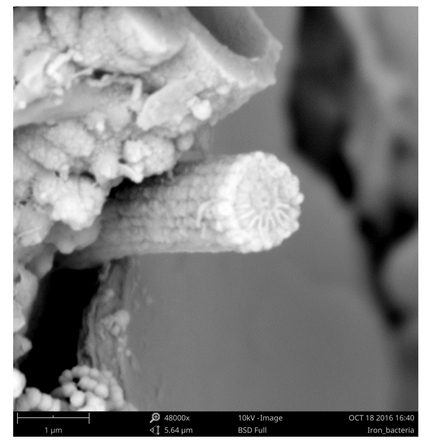

A

Day 0 | Day 5 | Day 12 | Day 18 | Day 26 | Day 33

Day 40 | Day 103 | Day 145 | Day 207 | Day 278 | Day 621

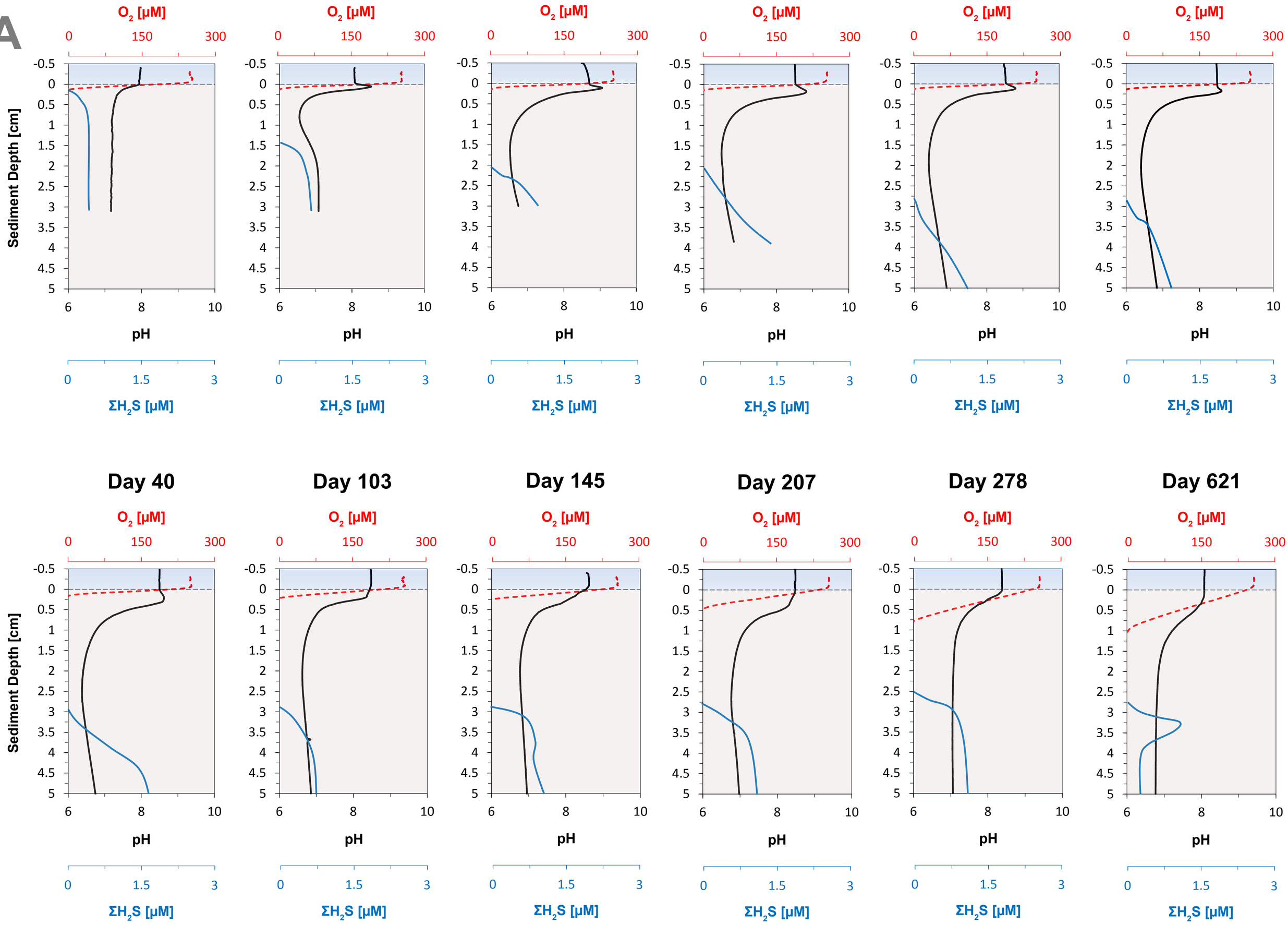

B

Day 0 | Day 5 | Day 12 | Day 18 | Day 26 | Day 33

Day 40 | Day 103 | Day 145 | Day 207 | Day 278 | Day 621

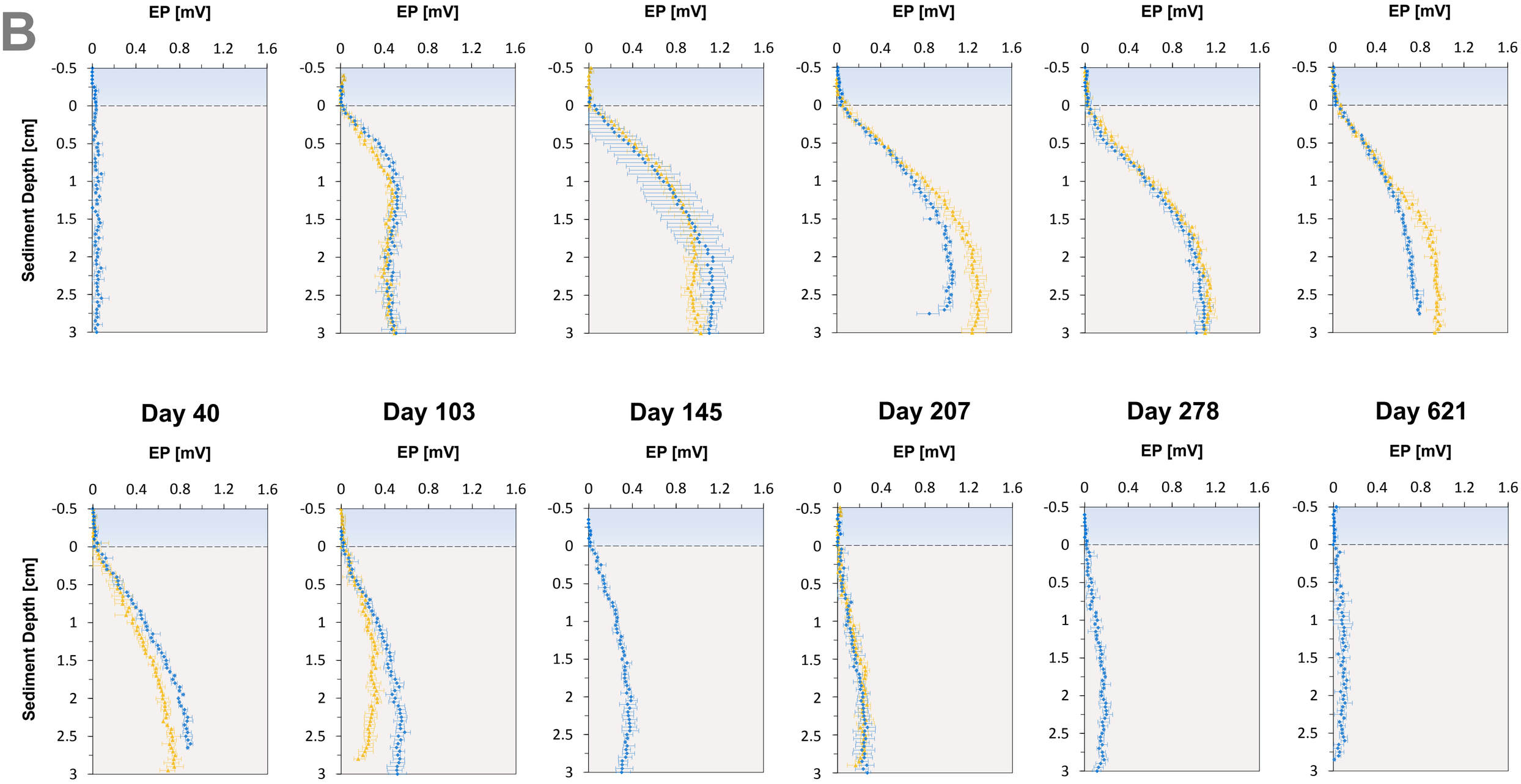

Depth Zonation [mm]

0
10
20
30
40

Day 0
Day 5
Day 12
Day 18
Day 26
Day 33
Day 40
Day 103
Day 146
Day 207
Day 278
Day 621

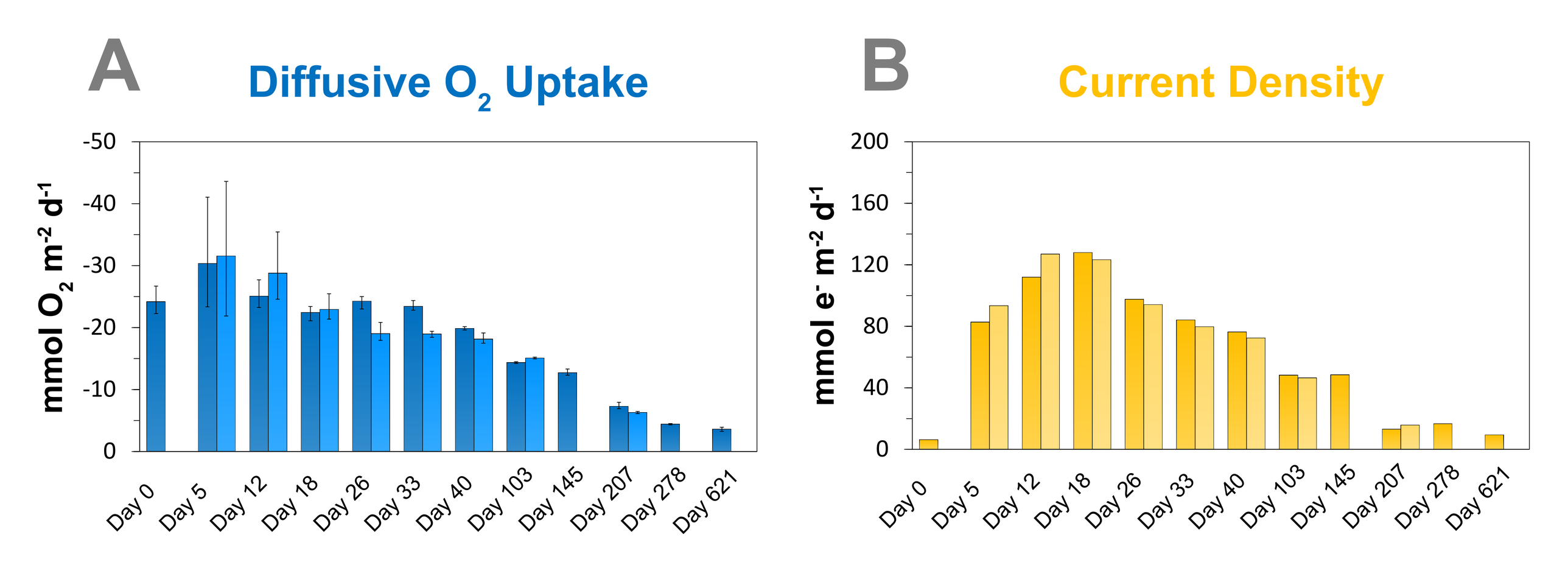
A
Diffusive O_2 Uptake
mmol O_2 m^{-2} d^{-1}
-50
-40
-30
-20
-10
0
Day 0
Day 5
Day 12
Day 18
Day 26
Day 33
Day 40
Day 103
Day 145
Day 207
Day 278
Day 621
B
Current Density
mmol e^- m^{-2} d^{-1}
200
160
120
80
40
0
Day 0
Day 5
Day 12
Day 18
Day 26
Day 33
Day 40
Day 103
Day 145
Day 207
Day 278
Day 621

Day 5 | Day 12 | Day 18 | Day 26 | Day 33 | Day 40 | Day 207 | Day 621 | Control

Depth [cm]

NH_4^+ [mM]

N/A

N/A

SO_4^{2-} [mM]

Fe^{2+} [mM]

Mn^{2+} [mM]

Ca^{2+} [mM]

HPO_4^{2-} [mM]

H_4SiO_4 [mM]

A

NH_4^+

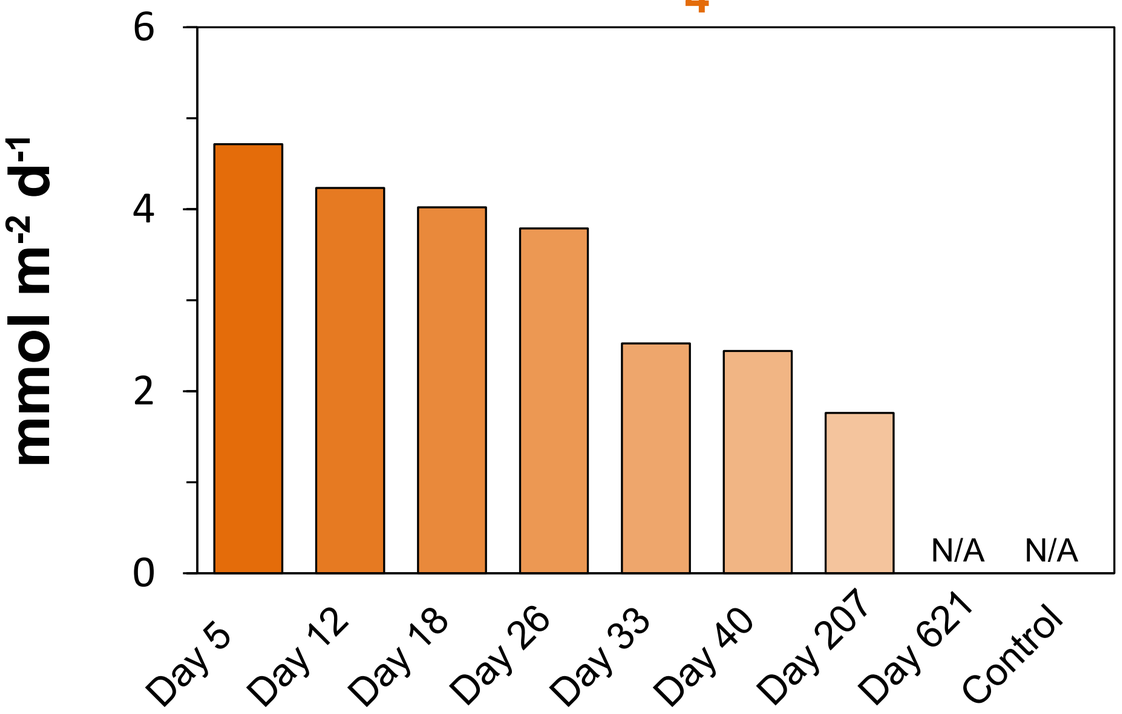

B

SO_4^{2-}

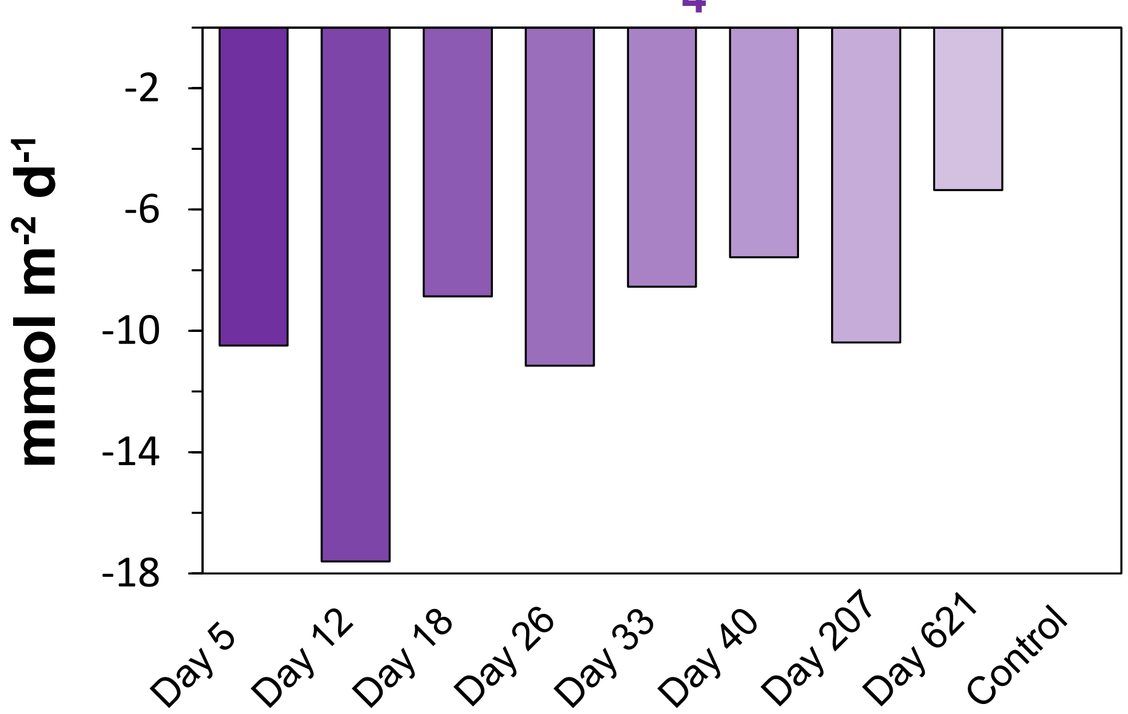

C

Fe^{2+}

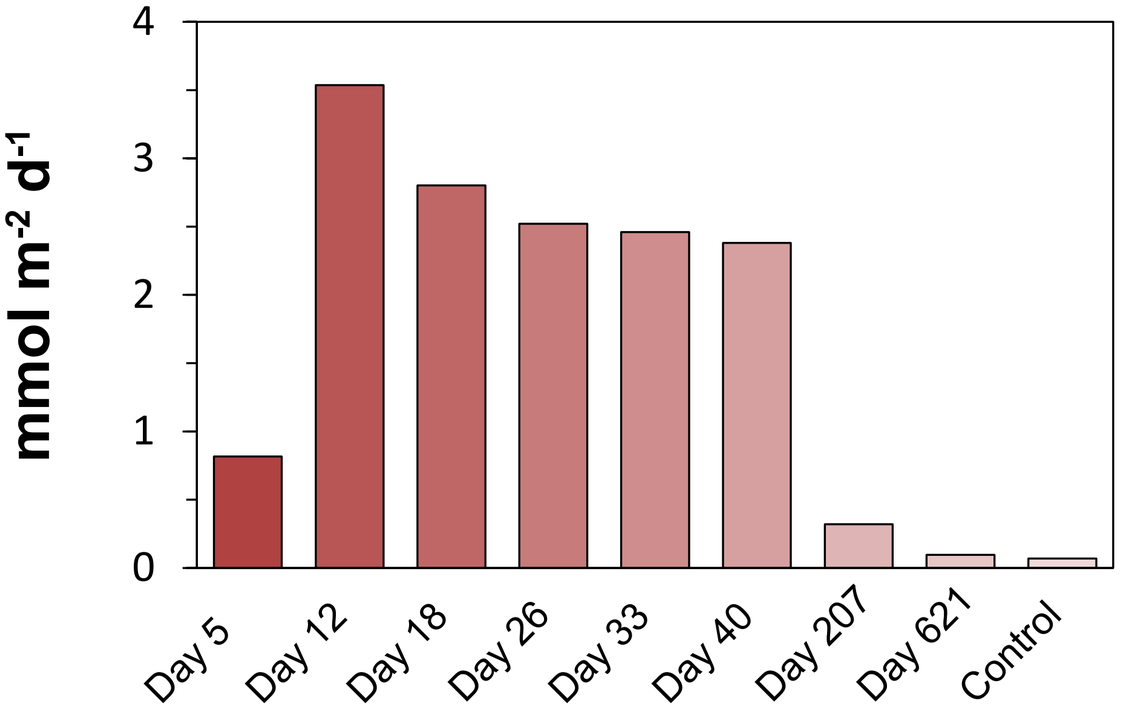

D

Mn^{2+}

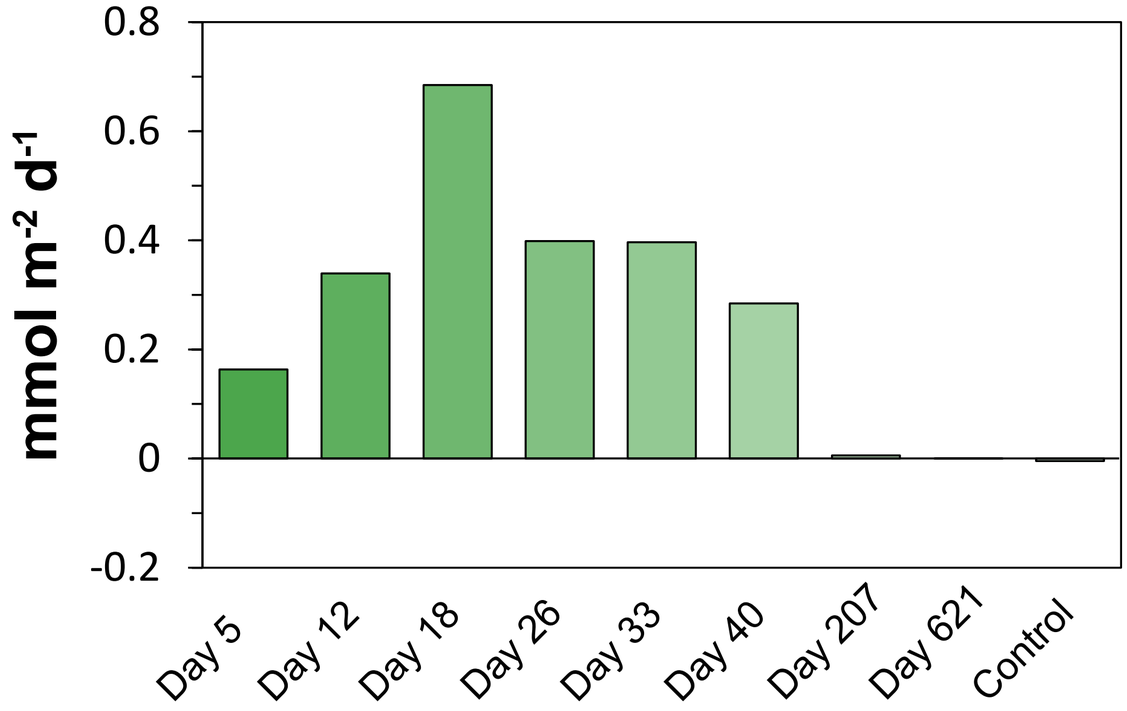

E

Ca^{2+}

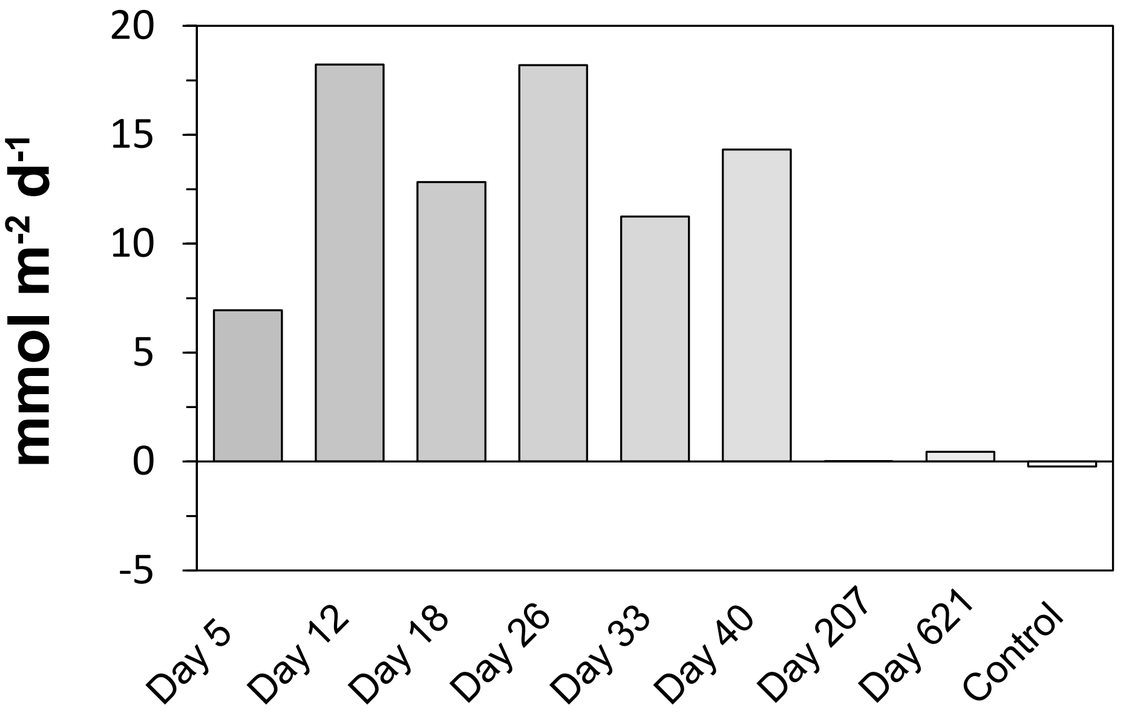

F

H_4SiO_4

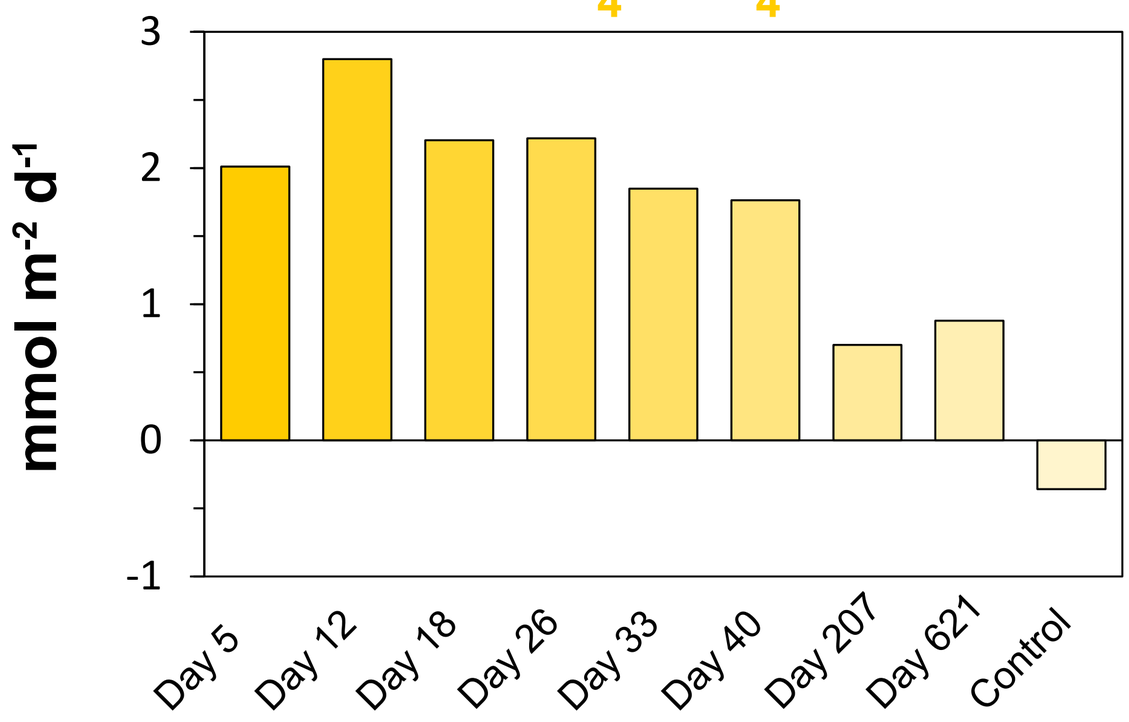

Day 5 | Day 12 | Day 18 | Day 26 | Day 33 | Day 40 | Day 207 | Day 621 | Control

Depth [cm]

Fe oxides (µmol g^{-1})

FeS (µmol g^{-1})

Siderite (µmol g^{-1})

Mn oxides (µmol g^{-1})

Metal bound P (µmol g^{-1})

Metal oxide bound Si (µmol g^{-1})

A

Black Sea Experiment
Cable bacteria

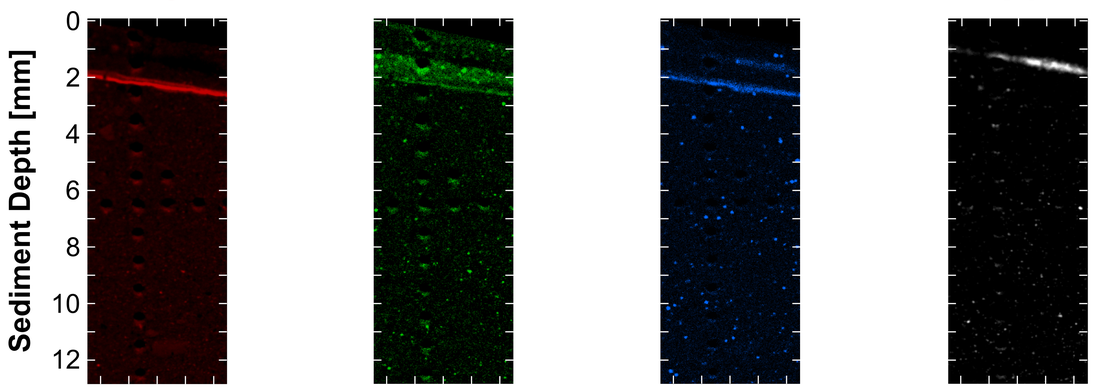

B

Gulf of Finland (GOF5)
Cable bacteria

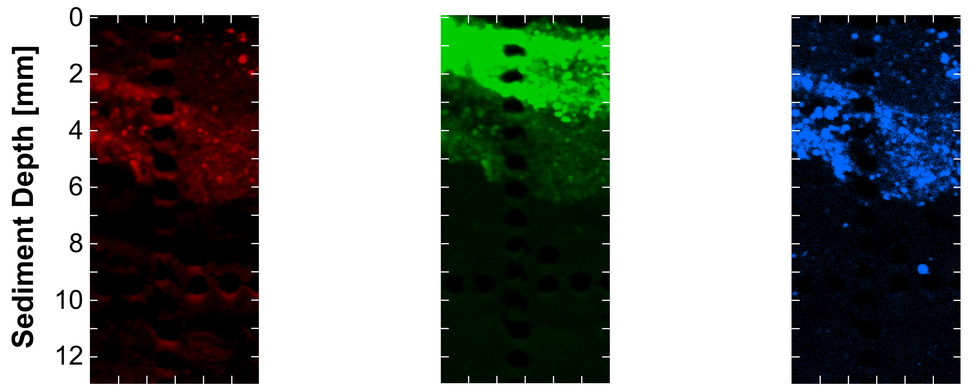

C

Lake Grevelingen in January
Cable bacteria

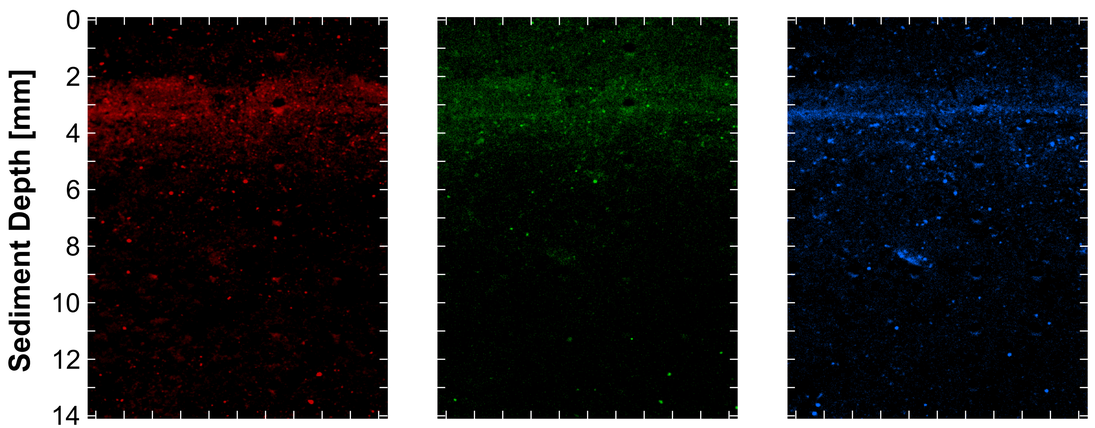

D

Lake Grevelingen in May
Macrofauna

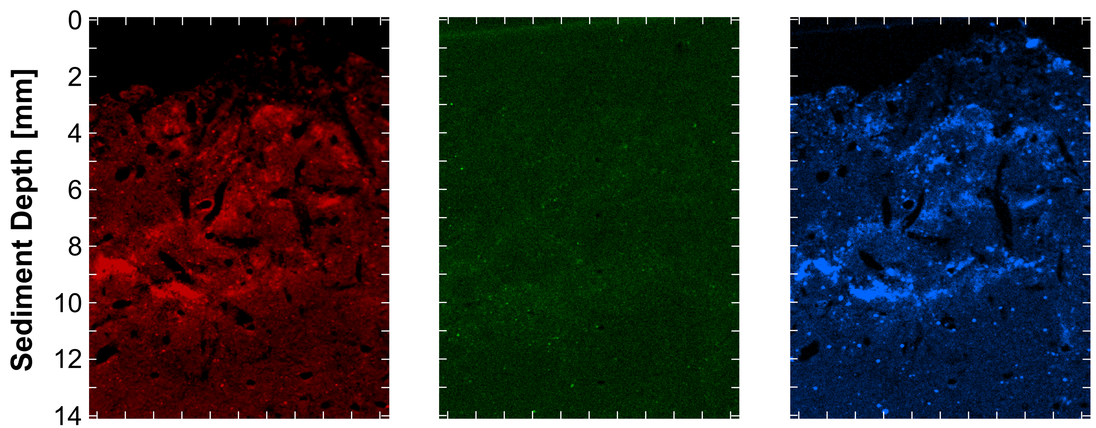

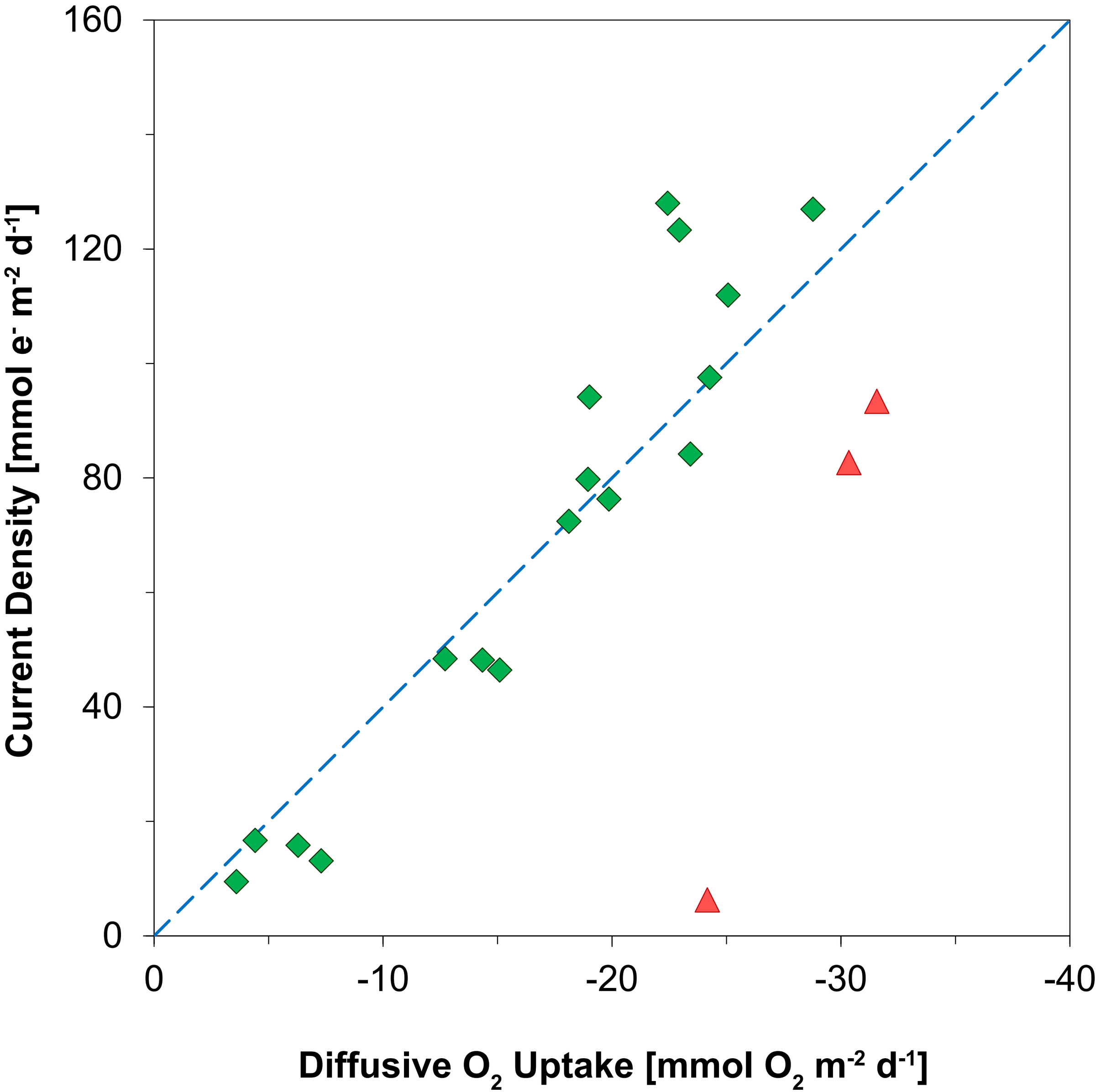
160
120
80
40
0
0
-10
-20
-30
-40
Current Density [mmol e⁻ m⁻² d⁻¹]
Diffusive O2 Uptake [mmol O2 m⁻² d⁻¹]

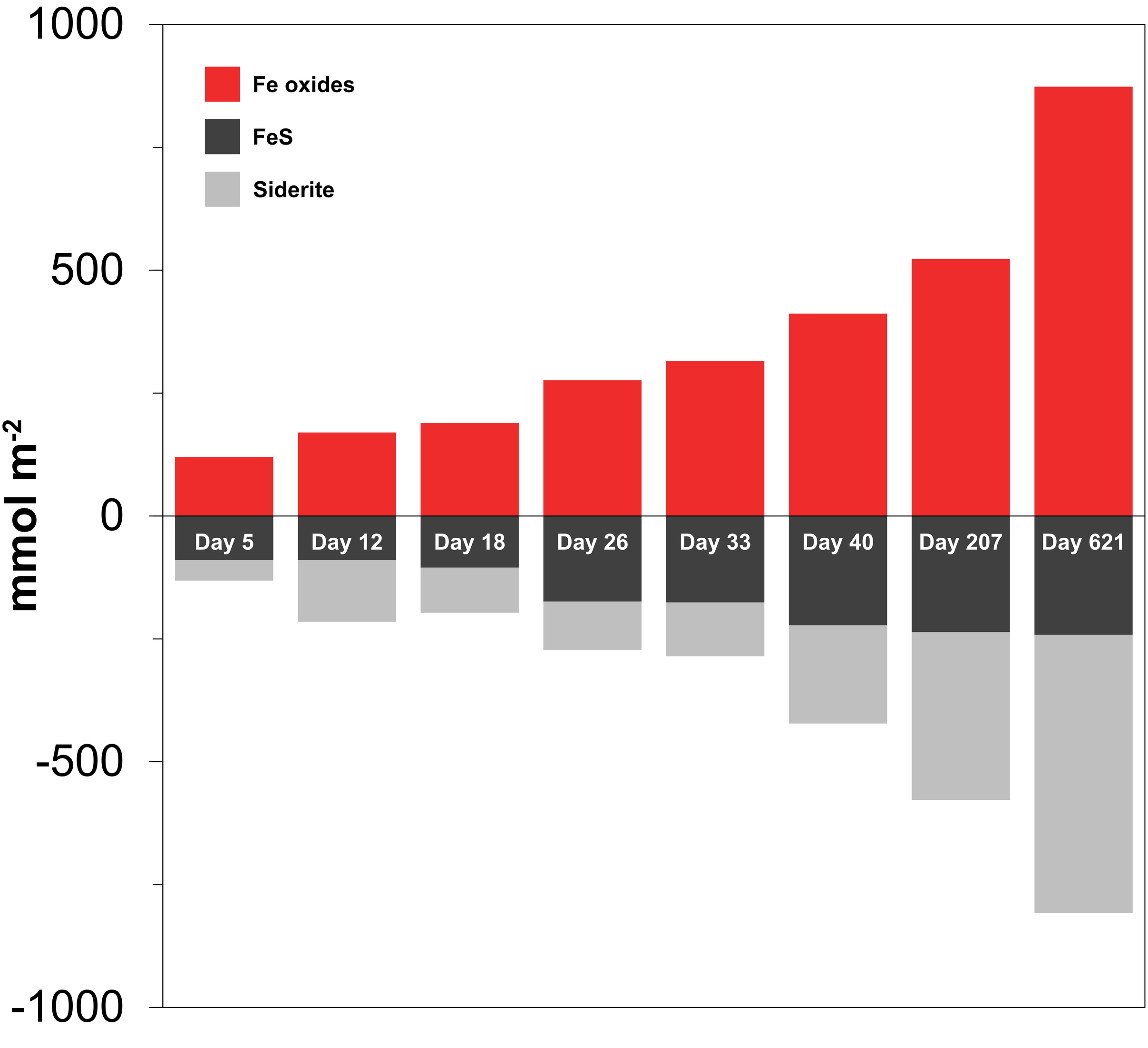
1000
500
0
-500
-1000
mmol m-2
Fe oxides
FeS
Siderite
Day 5
Day 12
Day 18
Day 26
Day 33
Day 40
Day 207
Day 621